PONTIFICIA UNIVERSIDAD CATOLICA DE CHILE

SCHOOL OF ENGINEERING

FATTY ACIDS CHARACTERIZATION DURING NON-ALCOHOLIC FATTY LIVER DISEASE USING MAGNETIC RESONANCE SPECTROSCOPY

ALINE CARVALHO DA SILVA XAVIER

Thesis submitted to the Office of Graduate Studies in partial fulfillment of the requirements for the Degree of Doctor in Engineering Sciences

Advisor:

MARCELO ANDIA KOHNENKAMPF

Santiago de Chile, July, 2020

PONTIFICIA UNIVERSIDAD CATOLICA DE CHILE
SCHOOL OF ENGINEERING

FATTY ACIDS CHARACTERIZATION DURING NON-ALCOHOLIC FATTY LIVER DISEASE USING MAGNETIC RESONANCE SPECTROSCOPY

ALINE CARVALHO DA SILVA XAVIER

Members of the Committee:

MARCELO ANDIA

FLAVIA ZACCONI

CRISTIAN TEJOS

CATALINA ARTEAGA DE CASTRO

DANIEL CABRERA

GUSTAVO LAGOS

Thesis submitted to the Office of Graduate Studies in partial fulfillment of the requirements for the Degree Doctor in Engineering Sciences

Santiago de Chile, July, 2020

To my beloved family: Montanha, Colina, Daniel, Márcio, Maria da Paz, Arthur, Andréa, Ana, Pedro, Juvany and Moacir.

AKNOWLEDGEMENTS

I wish to show my gratitude to the National Commission for Scientific Technological Research CONICYT-PCHA/Doctorado Nacional/2016-21160835 and Pontifícia Universidad Catolica de Chile for making this research possible.

I would like to thank my advisor Marcelo Andia for all knowledge shared with me, always with nice words and Flavia Zacconi for all the teaching, help and for being super friendly all the time. I would like to thank all my colleagues and friends at the Biomedical Imaging Center and, specially, Cristian Tejos, Sergio Uribe, Pablo Irarrázaval and Carlos Sing-Long for their advices in my study.

A special thanks to Catalina and Jeanine for teaching me so much in such a short time. I had a really nice time with them in Utrecht. I wish to express my deepest gratitude to Thomas, Begoña and Alkystis for all the support and great advices for my study.

I would like to recognize the invaluable assistance provided by Leonel, Claudio and Erick with the mass spectrometer and magnetic resonance equipment; and, by Nancy and Daniel with the animal models. A special thanks to Fabian for helping me with the fatty acid's extraction during many weekends and all the support as a friend.

Finally, a huge thanks to my family that always encourages me to do what makes me happy; to Daniel Torres, the love of my life, for all his patience and words of comfort; to my babies, Montanha and Colina, for their unconditional love (they are the reason I smile every day). The huge thanks go also to my "de sempre pra sempre" friends and to God, for everything I have and that I have already achieved in my life.

TABLE OF CONTENTS

Pág.

AKNOWLEDGEMENTS iv

LIST OF TABLES vii

LIST OF FIGURES viii

RESUMEN xiv

ABSTRACT xv

1. INTRODUCTION 1
   - 1.1 Thesis hypothesis 3
   - 1.2 Objectives 3
   - 1.3 Outline of thesis document 3
   - 1.4 Scientific contribution 4

2. EX-VIVO STUDY IN MICE MODEL FED WITH WESTERN DIET 5
   - 2.1 Introduction 5
   - 2.2 Subjects and methods 7
     - 2.2.1 Gas Chromatography with Mass Spectrometer 8
     - 2.2.2 Magnetic Resonance Spectroscopy 8
     - 2.2.3 Histology 9
     - 2.2.4 Correlation between GC-MS and MRS 10
     - 2.2.5 Statistical analyses 11
     - 2.2.6 Principal component analysis and clustering method 11
   - 2.3 Results 12
     - 2.3.1 Histology 13
     - 2.3.2 Gas Chromatography with Mass Spectrometer 15
     - 2.3.3 Magnetic Resonance Spectroscopy 17
   - 2.4 Discussion 22

3. EX-VIVO AND IN-VIVO STUDY IN MICE MODEL FED WITH CDAA DIET 25
   - 3.1 Introduction 25
   - 3.2 Subjects and methods 27

3.2.1 Animal diet 27
3.2.2 Ex-vivo study 28
3.2.3 In-vivo study 30
3.2.4 Statistical analysis 31
3.3 Results 31
3.3.1 Ex-vivo study 31
3.3.2 In-vivo study 35
3.3.3 Differences between the in-vivo and ex-vivo MRS 35
3.4 Discussion 38

4. TRANSLATIONAL STUDY WITH VOLUNTEERS AT 7 TESLA 42
4.1 Introduction 42
4.2 Subjects and methods 44
4.2.1 Data acquisition 44
4.2.2 Data processing and quantification 46
4.2.3 Statistical analysis 48
4.3 Results 49
4.3.1 Phantom measurements 49
4.3.2 In-vivo measurements 50
4.3.3 Intra-session repeatability 56
4.3.4 Inter-session reproducibility 57
4.3.5 Lipid unsaturation 58
4.4 Discussion 59

5. CONCLUSION 64

BIBLIOGRAFIA 66

LIST OF TABLES

Table 2.1. Gas-Chromatography-Mass Spectrometer (Clarus 680 PerkinElmer) configuration. 8

Table 2.2. Mice age, weight and the percentage of FAME in the liver for each group. The first group was fed with a chow diet, the second, third and fourth group was fed with a Western diet for 4, 10 and 24 weeks, respectively. 13

Table 4.1 Subjects' characteristics 44

LIST OF FIGURES

Figure 2.1. MRS simulation of a FAME with 18 carbons and 2 double bonds. The proton chemically equivalent are shown in numbers. 11

Figure 2.2. Hepatic histology results with hematoxylin/eosin (left) and picrosirius red (right). the average score and the range of steatosis, ballooning, inflammation, and fibrosis for each group is shown below the image. 14

Figure 2.3. Boxplot of NAS value for each mouse individually. NAS value varies between 0 and 8: A value bigger or equal to 5 means that the mouse has NASH.* $p<0.05$ (significant difference between groups) and NS (no significant difference between groups). 15

Figure 2.4. Change in Fatty Acids composition measured with GC-MS (mean±SD) for the four different groups of mice (control or chow diet, 4 weeks of Western diet, 10 weeks of Western diet and 24 weeks of Western diet). * $p<0.05$, ** $p<0.01$, ***$p<0.001$ (significant difference between groups) and NS (no significant difference between groups). 16

Figure 2.5. The relative contribution of each group of fatty acids: Saturated fatty acids (SFA: C14:0, C15:0, C16:0, C18:0), monounsaturated fatty acids (MUFA, C16:1, C18:1) and Polyunsaturated fatty acids (PUFA, C18:2, C18:3, C20:3, C20:4, C20:5 C22:6). 17

Figure 2.6. Areas under the curve (AUC) calculated with MestreNova V10.0. In red, the results of a control mouse with a chow-diet and in blue, a mouse with a Western diet for 24 weeks. 17

Figure 2.7. Change in the AUC of the 7 peaks measured in the 1H-MRS (mean±SD) for the four different groups of mice (control or chow diet, 4 weeks of Western diet, 10 weeks of Western diet and 24 weeks of Western diet). *$p<0.05$, **$p<0.01$, ***$p<0.001$ (significant differences between groups) and NS (No significant difference between groups). 18

Figure 2.8. Principal component analysis of GC-MS results (a) and MRS results (b) for all the groups of mice (control, 4 weeks Western diet, 10 weeks Western diet, and 24 weeks

Western diet). Agglomerative Hierarchical Clustering method to cluster the data of GC-MS (c) and MRS (d). X-axis id the principal component 1 and y-axis is the principal component 2. 20

Figure 2.9. Dendogram of the agglomerative Hierarchical Clustering obtained by the results of GC-MS (on the left) and MRS (on the right). The x-axis are the samples and y-axis are the distance. The black arrow shows the cut-point. 21

Figure 2.10. NAS value for each cluster found by PCA with the data from GC-MS and MRS. * p<0.05 (significant difference between groups) and NS (no significant difference between groups). 21

Figure 2.11. In-vivo MR spectra from a 9.4 Tesla in a mouse (red) and 7 Tesla in human (blue) showing that it is possible to identify all the seven peaks correspondent to the fat spectrum in the liver. 24

Figure 3.1. In-vivo voxel positioning to perform the STEAM sequence with TR/TM/TE= 2500/10/3ms, BW=5500 Hz, Nº points=2048, NSA=32, Voxel = 2x2x2 mm^2, total scan time = 1m20s. 31

Figure 3.2. (A) Mice´s weight, liver weight and percentage fatty acids in the liver for each group. (B) Liver histology sections of control group (I) and 4 weeks-diet (II) with hematoxylin/eosin, where macrovesicular steatosis, ballooning and inflammation can be visualised; and 10 weeks-diet (III) with Picrosirius Red, where fibrosis can be visualised. (C) Boxplot of NAS value for each mouse individually. *p < 0.05, **p < 0.01, ***p < 0.001 (significant differences between groups) and (D) the liver size comparing 4 weeks CDAA diet and the control group with chow diet. 33

Figure 3.3. (A) MRS spectra from control, mice fed with CDAA for 4 weeks and 10 weeks. (B) MRS data: change in the AUC of the 4 peaks measured in the 1H-MRS (mean $\pm$ SD). *p < 0.05, **p < 0.01, ***p < 0.001 (significant differences between groups). (C) The relative contribution of each group of fatty acids: Saturated fatty acids (SFA: C14:0, C15:0, C16:0, C18:0), monounsaturated fatty acids (MUFA, C16:1, C18:1) and

Polyunsaturated fatty acids (PUFA, C18:2, C18:3, C20:3, C20:4, C20:5 C22:6) for mice fed with CDAA diet *p < 0.05, **p < 0.01, ***p < 0.001 (significant differences between groups), ns means no significant difference. 34

Figure 3.4. (A) In-vivo results: Mice's weight (on the right) and the lipid content (on the left) for each mouse individually. Total lipid content (%) in the liver was calculated as L/(L + W) * 100, where W represents the amplitude of the water signal and L the total amplitude of the lipid signals. (B) In-vivo results from MRS. 36

Figure 3.5. (A) Graph showing the MRS in-vivo (blue) and ex-vivo (red). Residual water (*, at 4.7 ppm) and glycerol (**, around 4.2 ppm), are eliminated in the extraction process made for the ex-vivo analysis. (B) MRS results comparing metabolites in-vivo with ex-vivo. 37

Figure 3.6. The relative contribution of each group of fatty acids: Saturated fatty acids (SFA: C14:0, C15:0, C16:0, C18:0), monounsaturated fatty acids (MUFA, C16:1, C18:1) and Polyunsaturated fatty acids (PUFA, C18:2, C18:3, C20:3, C20:4, C20:5 C22:6) for mice fed Western diet. Data from Western diet came from a previous work of our group.*p < 0.05, **p < 0.01, ***p < 0.001 (significant differences between groups). The date was taken from Xavier et al, (2019b) 40

Figure 4.1. Spectra acquired in a phantom containing a lipid emulsion using (A) a conventional STEAM sequence and VAPOR water suppression, and (B and C) MC-STEAM without water suppression. In (B) the offsets for the MC pulses were +175 Hz and -175 Hz from the water frequency for odd and even scans, respectively (in-vivo settings), while in (C) the offsets for the MC pulses were +50 Hz and -50 Hz from the water frequency. All major lipid peaks in the upfield spectrum can be clearly identified within all spectra and are indicated in panel (A). The olefinic lipid signal at 5.3 ppm, however, can only be distinguished clearly in the VAPOR-STEAM spectrum (A) and in the MC-STEAM spectrum with the smaller offsets (C; olefinic lipid signal has a 180 degrees phase difference with the upfield signals). (D) Lipid methylene signal amplitude (expressed as a

percentage of the water signal) as a function of the B_1^+ used for the MC pulses. A B_1^+ above 15 μT in the region of interest is required for complete inversion of the methylene signal and thus to obtain the full signal amplitude in the difference spectra. 50

Figure 4.2. (A) Example of voxel (15 × 15 × 20 mm^3) positioning in the liver depicted on a transversal DIXON scan. The red voxel indicates the voxel positioning for the water frequency, while the white voxel indicates the shifted voxel for the lipid methylene frequency. (B-D) In-vivo liver spectra from the voxel indicated in (A) using MC-STEAM: (B) displays the downfield (blue) and upfield (red) inverted spectra (after individual phase correction, coil combination, frequency alignment and averaging); (C) shows the sum of the downfield and upfield inverted spectra (water spectrum); and (D) the difference (metabolite) spectrum..... 52

Figure 4.3. Comparison of in-vivo liver spectra from the voxel indicated in Figure 4.2A (all in the same subject) recorded using VAPOR-STEAM (left column) and MC-STEAM (right column) with free breathing reconstructed without frequency correction (A and B) and with frequency correction (C and D) and with synchronized breathing reconstructed without frequency correction (E and F) and with frequency correction (G and H). Peak assignments are indicated in panels (G) and (H). The peak at 3.22 ppm (not present in the phantom spectra) originates from choline containing compounds (total choline, tCho). Liver lipid content for this subject averaged over the different spectra was 2.3%. 53

Figure 4.4. Comparison of in-vivo liver spectra from another subject, with a lower liver lipid content as compared to the subject in Figure 4.3, recorded using VAPOR-STEAM (left column) and MC-STEAM (right column) with free breathing reconstructed without frequency correction (A and B) and with frequency correction (C and D) and with synchronized breathing reconstructed without frequency correction (E and F) and with frequency correction (G and H). Liver lipid content for this subject averaged over the different spectra was 1.0%. 54

Figure 4.5. (A) Average signal-to-noise ratio (SNR) for the lipid methylene peak (1.30 ppm) and (B) linewidth (LW) of the fitted lipid peaks for the 6 subjects for both scan sessions from acquisitions with VAPOR-STEAM with free breathing (light blue) and

synchronized breathing (dark blue), and MC-STEAM with free breathing (light green) and synchronized breathing (dark green). Results are shown for data reconstructed without (uniform colored bars) and with (colored bars with black hatches) frequency correction. For both SNR and LW, there was no significant difference between VAPOR and MC, but there was a significant interaction between the effects of reconstruction without and with frequency correction and measurements with free and synchronized breathing ($p=0.04$ and $p=0.03$ for SNR and LW, respectively). The significance signs in the figure represent the results of the Bonferroni corrected post-hoc tests for the pooled VAPOR and MC data. $*p<0.05$, $*p<0.01$. 55

Figure 4.6. Bland-Altman plots for comparisons of liver lipid content between scans with free breathing and synchronized breathing acquired with VAPOR-STEAM (A) and MC-STEAM (B) and for comparisons between scans with VAPOR-STEAM and MC-STEAM obtained with free breathing (C) and synchronized breathing (D). Spectra were reconstructed with frequency correction. Solid black line shows the bias from zero (thin black line) and dashed black lines mark ±1.96 SD. (A) absolute bias = 0.04%, CR = 0.42%, CV = 14.1%; (B) absolute bias = 0.05%, CR = 0.25%, CV = 8.3%; (C) absolute bias = 0.02%, CR = 0.45%, CV = 14.4%; (D) absolute bias = 0.06%, CR = 0.60%, CV = 20.0%..... 56

Figure 4.7. Bland-Altman plots of intra-session variability in liver lipid content measured with VAPOR-STEAM (A) and MC-STEAM (B) with synchronized breathing. Spectra were reconstructed with frequency correction. Solid black line shows the bias from zero (thin black line) and dashed black lines mark ±1.96 SD. (A) absolute bias = 0.06%, CR = 0.36%, CV = 12.2%; (B) absolute bias = 0.00%, CR = 0.29%, CV = 9.6%. 57

Figure 4.8. Bland-Altman plots of inter-session variability in liver lipid content measured with VAPOR-STEAM (A, C) and MC-STEAM (B, D) with free breathing (A, B) and synchronized breathing (C, D). Spectra were reconstructed with frequency correction. Solid black line shows the bias from zero (thin black line) and dashed black lines mark ±1.96 SD. (A) absolute bias = 0.01%, CR = 1.11%, CV = 37.1%; (B) absolute bias =

0.12%, CR = 0.68%, CV = 23.2%; (C) absolute bias = 0.06%, CR = 1.15%, CV = 39.5%; (D) absolute bias = 0.09%, CR = 0.90%, CV = 29.4%. 58

Figure 4.9. A,B: Bland-Altman plots of intra-session variability in unsaturation index (UI) of hepatic lipids measured with VAPOR-STEAM (A) and MC-STEAM (B) with synchronized breathing. Spectra were reconstructed with frequency correction. Solid black line shows the bias from zero (thin black line) and dashed black lines mark ±1.96 SD. (A) absolute bias = 0.00, CR = 0.15, CV = 51.7%; (B) absolute bias = 0.00, CR = 0.06, CV = 17.2%. C,D: UI versus liver lipid content for the 6 subjects for both scan sessions. Data were measured with VAPOR-STEAM (C) and MC-STEAM (D) with synchronized breathing and results of the two measurements acquired during one session were averaged. With MC-STEAM a significant negative correlation was observed, while the data acquired with VAPOR-STEAM did not indicate a clear relationship. 59

RESUMEN

Introducción: La enfermedad del hígado graso no-alcohólico (EHGNA) es la enfermedad hepática más común en el mundo y se está convirtiendo en una de las causas más frecuentes de trasplante hepático. Desafortunadamente, el único método disponible para determinar de manera confiable la etapa de esta enfermedad es la biopsia hepática, la cual es invasiva y riesgosa para los pacientes; y además no es representativa de todo el parénquima hepático. Algunos estudios sugieren que diferencias en la composición de la grasa hepática (i.e. los ácidos grasos) están relacionados a la progresión de esta enfermedad. **Objetivo:** El propósito de este estudio es investigar la composición de los ácidos grasos del hígado durante la progresión de la EHGNA mediante el uso de espectroscopía por resonancia magnética (ERM), un método potencialmente no-invasivo. **Metodología:** Hemos realizado un estudio de ERM ex-vivo de manera de comparar nuestros resultados con los métodos invasivos estándares. Este estudio ex-vivo se realizó con 2 modelos murinos alimentados con dieta Western y CDAA. Luego, realizamos un estudio in-vivo, y utilizamos el estudio ex-vivo como validación. Finalmente, probamos la viabilidad de realizar nuestras técnicas en resonadores clínicos con voluntarios usando un equipo de 7 Tesla. **Resultados:** La composición de los ácidos grasos del hígado cambia a medida que la EHGNA progresa de esteatosis a esteatohepatitis, pero permanece invariable durante las diferentes etapas de esteatohepatitis. Utilizando el análisis de componentes principales en los datos de ERM, identificamos los tres grupos clínicos más relevantes: normal, esteatosis y esteatohepatitis. Estos resultados mostraron muy buena concordancia con los resultados de los métodos invasivos estándares. Con la ERM in-vivo, en voluntarios, comprobamos la viabilidad de identificar los peaks de los ácidos grasos en el espectro hepático. **Conclusión:** Se demostró en modelos animales que es posible detectar la progresión de la esteatosis simple a esteatohepatitis utilizando ERM hepática y que este método tiene potencial para ser utilizado en la clínica, en humanos y potencialmente reemplazar la biopsia hepática.

Palabras Claves: Enfermedad del hígado graso no alcohólica; Espectroscopia por resonancia magnética; Ácidos grasos

ABSTRACT

Introduction: Non-alcoholic fatty liver disease (NAFLD) is the most common liver disease in the world and it is becoming one of the most frequent causes of liver transplantation. Unfortunately, the only method available to reliably determine the stage of this disease is liver biopsy, which is invasive and risky for patients; and it is also not representative of the entire liver parenchyma. Some studies suggest that differences in the composition of liver fat (i.e. fatty acids) are related to the progression of this disease. **Objective:** The purpose of this study is to investigate the fatty acid composition of the liver during the progression of NAFLD by using magnetic resonance spectroscopy (MRS), a potentially non-invasive method. **Methodology:** We have conducted an ex-vivo MRS study to compare our results with standard invasive methods. This ex-vivo study was performed with 2 murine models fed with Western and CDAA diet. Then we performed an in-vivo study and used the ex-vivo study as validation. Finally, we tested the feasibility of performing our techniques with volunteers, using 7 Tesla MRS. **Results:** The liver fatty acid composition changes as NAFLD progresses from steatosis to steatohepatitis, but remains unchanged during the different stages of steatohepatitis. Using principal component analysis on MRS data, we identified the three most relevant clinical groups: normal, steatosis, and steatohepatitis. These results showed very good agreement with the results of the standard invasive methods. With in-vivo MRS, we tested the feasibility of identifying fatty acid peaks in the liver spectrum in volunteers. **Conclusion:** It was demonstrated in animal models that it is possible to detect the progression from simple steatosis to steatohepatitis using liver MRS and that this method has the potential to be used clinically, in humans, and potentially replace liver biopsy.

Keywords: Non-alcoholic fatty liver disease; Magnetic resonance spectroscopy; Fatty acids

1. INTRODUCTION

Non-alcoholic fatty liver disease (NAFLD) is characterized by the accumulation of intracellular lipids in the liver in the absence of excessive alcohol consumption. The spectrum of this disease starts with a simple steatosis; it may progress to non-alcoholic steatohepatitis (NASH) with different degrees of inflammation, and with or without fibrosis; and ultimately, cirrhosis and hepatocellular carcinoma (Friedman et al, 2018). NAFLD is the most common liver disease in the world and it is becoming one of the most frequent cause of liver transplantation in United States (Younossi et al, 2016), (Younossi et al, 2018). Unfortunately, the gold standard to confirm the stage of NAFLD is the histology from the liver biopsy, but it is invasive and risky for the patients (Friedman et al, 2018). It has been estimated that between 30% to 40% of patient with steatosis evolves to NASH, and between 10 to 25% of them will develop cirrhosis within 10 years. Therefore, it is needed a non-invasive method that can accurately determinate the stage of the diseases and the risk of progression (Neumann & Cohem, 2014).

Currently, the methods for NAFLD diagnosis are based on the estimation of the total amount of fat infiltration in the liver, and this does not have a good correlation with clinical progression (McClain et al, 2007). The total fat in the liver does not consider the differences in its composition (i.e., fatty acids concentration), which has been proposed as a better method to discriminate between this group of diseases (Puri et al, 2007), (Araya et al, 2004), (Xavier et al, 2019a). The great advantage of determining the progression of the disease based on the fatty acids (FA) is the possibility to associate the results of the FA concentrations into the results of a non-invasive exam performed with magnetic resonance spectroscopy (MRS), which allows to determine the structure of organic substances (Permutt et al, 2012).

To better understand the progression of the fatty liver disease, many researchers prefers to work with mice models since the NAFLD can take long time to progress in humans and, also, for ethical reasons, since it is not possible to perform many biopsies during the time the person has NAFLD (Hebbard & George, 2011).

There are many murine models of NAFLD; they are basically divided into two big groups (Machado et al, 2015), (Hariri & Thibault, 2010), (Sanches et al, 2015), (Lau et al, 2017), (Van Heck et al, 2017), (Hebbard et al, 2011): diet models and genetic models. Within the first group, there are diets more like humans diet, rich in fat, that generates metabolic disorders and increases the accumulation of fat in the liver (ex: high-fat diet and Western diet), and there are diets which the focus is in generating inflammation and liver injury such as CDAA (*choline-deficient*, l-amino acid-defined) (Van Heck et al, 2017) and MCD (methionine and choline-deficient) (Machado et al, 2015) diets. In this thesis we are going to use wild-type mice fed with two diets. The first diet will be the "Western Diet", with a "metabolic" effect that resemble better what happen in human patient with obesity and metabolic syndrome, however it is a long intervention and usually the transition to NASH is very slow (Sanches et al, 2015). The second diet will be the "CDAA Diet", that have an acute inflammatory effect over the liver, and accelerate the transition from steatosis to NASH and cirrhosis (Van Heck et al, 2017).

In this thesis we propose to use Proton Magnetic Resonance Spectroscopy (^{1}H-MRS) to study the intrahepatocyte fatty acid composition during the progression of the NAFLD with the aim to accurately characterise the stages of this disease progression based on the non-invasive information obtained from the MRS.

^{1}H-MRS uses the magnetic property of the atom's nucleus when it is expose to a static magnetic field and then excited by a Radio-frequency pulse to produce the spectra and to give metabolic information in a graphic of frequency versus amplitude (De Graaf, 2019). We test our hypothesis using the two murine models described before, and we performed ex-vivo and in-vivo studies in order to validate our findings with the current gold-standards: GC-MS (the gas chromatography with a mass spectrometer) and histology. Additionally, we adapt our methodology to test the feasibility to be used in humans using a clinical 7T MR scanner in collaboration with the University Medical Center Utrecht (UMCU), The Netherland.

1.1 Thesis hypothesis

The progression of the NAFLD is related to the type of fatty acids stored in the hepatocyte, besides the total amount of fat in the liver; and the composition of the fatty acids could be inferred by using Magnetic Resonance Spectroscopy.

1.2 Objectives

1- To characterise the intracellular composition of the liver fatty acids using ^{1}H-MRS during the progression of NAFLD in a mice model fed with Western diet.
2- To characterise the intracellular composition of the liver fatty acids using in-vivo and ex-vivo MRS in a mice model fed with CDAA diet.
3- To improve the available technique to perform high-resolution MRS in human liver at high field and the feasibility to obtain all the peaks needed to perform the fatty acids analysis.

1.3 Outline of thesis document

This thesis will be presented in five chapters.
In Chapter 2, we present the result of the first objective, that is to investigate the intracellular composition of the liver fatty acids using MRS during the progression of NAFLD in a mice model fed with Western diet, with the aim of identifying non-invasive classifiers of NAFLD progression from steatosis to NASH. Our findings will be validated with the current invasive gold-standard methods (histology, GC-MS). This objective will be explained in detail in Chapter 2.
In Chapter 3, we present the result of the second objective, that is to compare the liver fatty acids composition in the progression of NAFLD with a mice model using a CDAA diet during the time they develop NASH. In order to do it, we have performed an in-vivo and ex-vivo analysis to validate each step of the methodology. This objective will be explained in detail in Chapter 3.

In Chapter 4, we present the result of the third objective, which was to improve an existent method to perform MRS in human liver by using a 7 Tesla MR scanner in order to obtain a spectrum with enough resolution to analyse all peaks correspondent to fatty acids. This objective will be explained in detail in Chapter 4.
In Chapter 5 we summarised the main conclusions and limitations of this thesis and propose future works.

1.4 Scientific contribution

This thesis generated three articles, one is already published in the journal RSC advances (Xavier et al, 2019b), the second one has been accepted for publication in the journal NMR in Biomedicine (Xavier, 2020a), and the third one has been recently submitted (Xavier, 2020b). Additionally, thirteen abstracts have been presented in poster or oral format in international conferences of the ISMRM (The International Society for Magnetic Resonance in Medicine) and ESMRMB (The European Society for Magnetic Resonance in Medicine and Biology); and one conference abstract has been published as paper in the IFMBE (International Federation of Medical and Biological Engineering) proceedings (Xavier 2019a).

This thesis has received the valuable support of the following grants:

- CONICYT-PCHA/ Doctorado Nacional/ 2016-21160835.
- Millennium Science Initiative of the Ministry of Economy, Development and Tourism, grant Nucleus for Cardiovascular Magnetic Resonance and Millennium Nucleus Center for Discovery of Structures in Complex Data
- FONDECYT 1180525, 11171001, 1191145 and 11160728.
- FONDEQUIP EQM120021 and EQM150020
- Nederlandse Organisatie voor Wetenschappelijk Onderzoek (NWO) (project 040.11.634)

2. EX-VIVO STUDY IN MICE MODEL FED WITH WESTERN DIET

This chapter is based on the article: **Xavier, A.**, Zacconi, F., Gainza, C., Cabrera, D., Arrese, M., Uribe, S., ... & Andia, M. E. (2019). Intrahepatic fatty acids composition as a biomarker of NAFLD progression from steatosis to NASH by using ^{1}H-MRS. *RSC Advances*, *9*(72), 42132-42139

2.1 Introduction

Non-alcoholic fatty liver disease (NAFLD) is characterized by the accumulation of intracellular fatty acids in the liver in the absence of excessive alcohol consumption. The spectrum of this disease starts with a simple steatosis; it may progress to non-alcoholic steatohepatitis (NASH) with different degrees of inflammation, and with or without fibrosis; and ultimately cirrhosis and hepatocellular carcinoma (Friedman et al, 2018). NAFLD is strongly associate with obesity and metabolic syndrome, which are the most common non-transmissible chronic diseases in Western countries (Friedman et al, 2018), (Wiliams & Taylor-Robinson, 2016).

Research performed in 2015 with a sample of 8,515,431 patients from 22 countries showed that 25% of the total population in the world suffers from NAFLD (Younossi et al, 2016). According to statistics, about 30% - 40% of people with steatosis develop NASH. Moreover, 10% - 30% of them develop cirrhosis, which could progress to hepatocellular carcinoma (Neumann & Cohem, 2014).

Currently, there are no specific biomarkers that can predict this “bad progression” of NAFLD. Most of the current available diagnosis methods mainly focus on estimating the total amount of fat stored in the liver using ultrasound (US), computed tomography (CT) or magnetic resonance imaging (MRI). However, these methods have some drawbacks: US does not work properly in obese patients, CT uses ionizing radiation and none of these methods can recognize either inflammation or early stages of fibrosis. In addition, it is necessary to detect the disease in NASH stages while the disease is reversible (Perry et al, 2015). Therefore, the only method that can reliably determine the stage of this disease is a

biopsy with a histological evaluation, however, it is invasive and risky for patients (Ahmed, 2015), (Permutt et al, 2012), (Reeder et al, 2011).

In an attempt to develop biomarkers correlated with the progression of the disease, previous studies have characterized the fatty acids (FA) stored in the intracellular lipids in the liver by using gas chromatography with mass spectrometer (GC-MS), and they have identified some changes in the FA profile when comparing healthy livers, livers with steatosis, and livers with steatohepatitis (Yamada et al, 2015), (Guo & Zhang, 2011), (Puri et al, 2007), (Araya et al, 2004). Araya et al. (2004) found a decrease in polyunsaturated fatty acids (PUFA), while the saturated fatty acids (SFA) and the monounsaturated fatty acids (MUFA) had no significant changes between healthy patients and patients with steatosis. This study also found a decrease of the long chain polyunsaturated fatty acids between healthy patients and patients with steatosis, and between patients with steatosis and patients with steatohepatitis. Additionally, the same conclusion was found by Puri et al. (2007).

Although the analysis of the lipid composition opens an interesting field for the diagnosis of fatty liver progression, it still requires a biopsy, so its routine use is limited. On the other hand, magnetic resonance spectroscopy (MRS) provides a non-invasive technique that allows to determine the structure of organic substances (Permutt et al, 2012). The idea of defining a classifier using MRS emerges due to the need to find a way to replace biopsy with a non-invasive method that can classify NAFLD based on the composition of different fatty acids stored in the liver.

Previous studies have shown that it is possible to associate the results of MRS with those obtained from GC-MS. Unfortunately, those studies considered only fatty acids with 14, 16 and 18 carbons and not fatty acids with long chain, which seems to have a big relevance in the NAFLD progression (Knothe & Kenar, 2004), (Guillen & Ruiz, 2003), (Miyake et al, 1998), (Ren et al, 2008). Furthermore, studies that emphasize the importance of fatty acids on the liver have analyzed it in-vivo with MRS but have not correlated their results with the true amount of fatty acids as no biopsy was performed (Hamilton et al, 2011), (Longo et al, 1995), (Johnson et al, 2008), (Lee et al, 2013).

The purpose of this study is to investigate and compare the intracellular composition of the liver fatty acids using histology, GC-MS, 9.4T ^{1}H-MRS during the progression of NAFLD in a mice model fed with Western diet, with the aim of identifying non-invasive biomarkers of NAFLD progression to NASH.

2.2 Subjects and methods

All experiments were approved by the Scientific Ethics Committee for the care of animals and the environment of the Pontificia Universidad Católica de Chile (number: 170614002).

We fed a group of C57BL/6 male mice with Western diet (AIN76A, Test Diet) for 4 weeks (n=6), 10 weeks (n=6) and 24 weeks (n=6). The Western diet has 4.49 kilocalories per gram, and the calories come from: fat (40%), protein (15.8%), and carbohydrate (44.2%). We also fed a group (n=6) with a chow diet (500l*, Labdiet) with 3.36 kilocalories per gram, and the calories come from: fat (13.4%), protein (30%), and carbohydrate (57%). The Western diet is a model of "Western fast food" diet characterized by high calories, high cholesterol, and high fructose content (Krishnan et al, 2017).

At the end of the diet intervention, the mice were anesthetized with ketamine/xylosine, and the livers were harvested. A portion of the liver was used for histology analysis. The remaining liver was divided into two portions that were analyzed independently. We extracted the intracellular FA using a protocol adapted by Folch et al. (Folch et al, 1957), proceeded by an esterification process to obtain fatty acids methyl esters (FAME) since they are more stable (do not form hydrogen bridges). It is important to comment that the quantity of FA is the same as FAME. Finally, those FAME were analyzed using a 9.4T MRS and GC-MS.

Previous studies (Xavier et al, 2019a) were performed and allowed the conclusion that 300 mg of liver was required since, after the extraction in healthy mice, we obtained 5 mg of FAME and that is the minimum amount of sample required to perform a ^{1}H-MRS with enough signal-to-noise ratio (SNR). For the GC-MS, 2 mg of FAME is enough.

2.2.1 Gas Chromatography with Mass Spectrometer

FAME were analyzed by using GC-MS (Perkin-Elmer, Clarus 680) equipped with HP-Innowax capillary column (length 25 meters, 0.2 mm internal diameter, 0.2 mm film). Additional configuration of GC-MS is found in Table 2.1. Data register was in SCAN mode and peak integration was obtained by the TurboMass Training 2016 PRO software.

FAME were identified by comparing retention times to known standards and by matching them up with the mass spectra from NIST library (National Institute of Standards and Technology, USA).

The mass of each FAME (in μg) was calculated according to the integration area of corresponding peak and the relation with the integration area of the internal standard (C19:0) added to the sample (50 μg). Fatty acids composition was defined as the percentage of individual fatty acids in respect of its total.

Table 2.1. Gas-Chromatography-Mass Spectrometer (Clarus 680 PerkinElmer) configuration.

Injector temp.	Oven ramp	Sample injection	Electron impact
220 ºC	150 ºC x 1 min 15 ºC/min to 200 ºC 200 ºC x 5 min 12 ºC/min to 260 ºC	Split mode (1:20) Helium at 1 ml/min (constant flow)	Ionization potential of 70eV

2.2.2 Magnetic Resonance Spectroscopy

The ^{1}H-MRS spectra of the FAME were obtained in a Bruker Avance spectrometer operating at 9.4 Tesla with the acquisition protocol Zg30 (30 degrees in z axis).

We took a known value in mg of FAME from each sample and added 700 μl of CDCl3 that has a small proportion of tetramethylsilane (TMS) as an internal reference. This mixture was introduced into a 5 mm diameter tube. The spectra acquisition was made with Topspin V3.0 and the parameters were: spectral width 8012.820 Hz, relaxation delay 1 s, number of scans 16, acquisition time 2.045 s, flip angle 30º to avoid T1 relaxation effects and total acquisition time 48.72 s (number of scans × [time between pulses + acquisition time]). The experiment was conducted at 25 ºC. The spectra were analyzed using

MestreNova Version 10.0. First, the spectra were centered (TMS in 0 ppm); then we calculated the area under the curve (AUC) of all seven peaks corresponding to fatty acids and finally, we normalized the AUC by the total amount of fatty acids. The fatty acids peaks used were: methyl terminal protons (-CH_3, approximately 0.9 ppm); bulk methylene protons ((-CH_2-)$_n$, approximately 1.3 ppm); β-methylene protons (-COO-CH_2-CH_2-, approximately 1.6 ppm); allylic protons (-CH_2-CH=CH-CH_2-, approximately 2.0 ppm) α-methylene protons (-COO-CH_2-, approximately 2.2 ppm); diallylic protons (–CH_2=CH–CH_2–CH=CH_2-, approximately 2.8 ppm) and olefinic internal protons (–CH=CH–, approximately 5.3 ppm).

2.2.2 Histology

Liver sections from mice livers were routinely fixed in 10% of formalin and embedded in paraffin. Then 5μm tissue sections were stained with hematoxylin/eosin, oil red and Picrosirius Red, as described previously (Cabrera et al, 2017). Whole slide imaging was obtained using the Aperio Digital Pathology Slide Scanner (Leica Biosystems) allowing us to study the entire left lateral lobe. Histopathological analyses were performed by a blinded pathologist starting from three full cross-sectional slides obtained from distal, medial, and proximal regions derived from the left lateral lobe. The blinded trained pathologist utilized the NAFLD Activity Score (NAS) by using the method proposed by Kleiner et al. (2005).

The score of steatoses vary between 0 and 3, the score of ballooning vary between 0 and 2, the score of inflammation vary between 0 and 3, and the score of fibrosis vary between 0 and 4. The NAS is the sum of steatosis, ballooning and inflammation scores. It can vary between 0 and 8. A NAS score less than 3 means no NASH, while a score higher than 4 means NASH. Scores of 3 or 4 means indeterminate.

2.2.3 Correlation between GC-MS and MRS

The MRS allows us to determine the structure of an organic substance. The spectrum shows the signals in a graph of frequency (ppm) versus intensity in arbitrary units. Each set of chemically equivalent protons originates a signal in such a way that the number of signals in a spectrum indicates the amount of different kinds of protons in a substance. The chemical shift is a measure of how far away the signal is from the reference signal of tetramethylsilane (TMS). The greater the displacement with respect to the TMS (0 ppm) is, the closer the proton is to an environment where there is an electronegative group (Yurkanis, 2008).

The GC is the gold standard to characterize fatty acids. The mixture containing all the fatty acids methyl esters is introduced in a GC-MS where it is warmed, and the fatty acids start to separate from each other by their volatility and polarity (Poole, 2008).

There are many types of FA in the liver of a human being. All of them generate just seven peaks corresponding to the chemical equivalent protons. Figure 2.1 shows an example of a FAME with 18 carbons and 2 double bonds in the signal of the MR spectroscopy.

Therefore, MRS does not detect the quantity of the fatty acids directly, but it is possible to assume that, if we have a change in fatty acids profile, we will have a change in the metabolites detected by MRS.

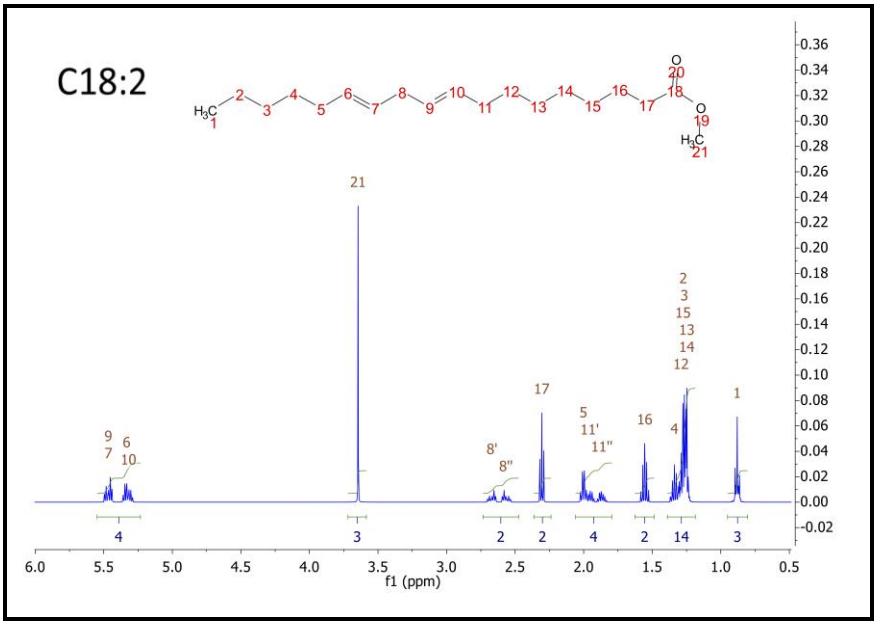

Figure 2.1. MRS simulation of a FAME with 18 carbons and 2 double bonds. The proton chemically equivalent are shown in numbers.

2.2.4 Statistical analyses

All statistical analyses were performed using Prism 6 (GraphPad Software Inc, La Jolla, CA). The data have normal distribution as confirmed by Shapiro-Wilk test. All graphs were plotted as mean ± standard deviation or boxplot. To compare between 3 or more groups, the ANOVA test was performed followed by a Bonferroni post-hoc test. A P-value <0.05 was considered to indicate statistical significance.

2.2.5 Principal component analysis and clustering method

Even though mice are fed with the same amount of diet for a fixed period, the disease may progress differently in each mouse. In order to identify changes in fatty acids and metabolites, we have used principal component analysis (PCA) to visualize the stage of the disease in each mouse, and a clustering method to group the mice according to their GC-MS and MRS measurements.

PCA is a data analysis technique that is used to represent a large set of data samples with a reduced set of features that explain most of the variability in the original set. These features, called principal components, are determined by finding linear combinations of the data samples that explain the largest variability in the dataset. Therefore, the first principal component corresponds to the direction of maximum possible variance, whereas the second explains the maximum remaining variance and so on (James et al, 2013). By considering a small number of principal components, we can visualize the data and determine if there is a natural distribution of the measurements performed on each mouse that correlates to their disease progression. The entry values for the PCA was all the lipid peaks found by MRS and all the fatty acids found by GC-MS. Pandas and Sklearn libraries were used in the Jupyter application and the code was programmed in pyton3 language.

To determine if the distribution of GC-MS and ^{1}H-MRS data has itself some structure from which we can infer the presence or progression of the disease, an agglomerative hierarchical clustering method was applied. Agglomerative hierarchical clustering is a "bottom-up" approach; each data point is initially considered to be a cluster, and data points are grouped together at each step according to some criterion. At the end of the procedure we obtain several potential groupings of the data, with a decreasing number of clusters (James et al, 2008). For our analysis, the data points are grouped according to their Euclidean distance and Ward's linkage function (Ward, 1963). This choice promotes that at each step, among all possible choices, pairs of clusters are merged in order to minimize the variation within the resulting cluster with respect to all other possible choices.

2.3 Results

Mice fed with Western diet increased their weight and accumulated fat in the liver. Table 2.2 shows the mice weight, liver weight and the total liver FAME content (mass of FAME/total liver sample, %) for each group at 4 time points: 0, 4, 10 and 24 weeks since diet intervention. By comparing the total amount of fatty acid in two

portions of the same liver (that were analyzed independently before averaging), we identified a maximum difference of 5%.

Table 2.2. Mice age, weight and the percentage of FAME in the liver for each group. The first group was fed with a chow diet, the second, third and fourth group was fed with a Western diet for 4, 10 and 24 weeks, respectively.

Mice group	Mice Age (weeks)	Mice Weight (g)	Liver Weight (g)	Weight of FAME/total liver sample, %
Chow-diet (control)	16	26.63±1.33	1.22±0.07	3.07±0.65
Western diet for 4weeks	16	28.27±2.76	1.14±0.08	5.84±2.11
Western diet for 10weeks	22	36.23±6.24	1.61±0.56	12.68±4.28
Western diet for 24weeks	36	46.23±2.12	3.32±0.48	23.62±2.54

2.3.1 Histology

Figure 2.2 shows the results of histology for each group. Besides that, the average score and the range of steatosis, ballooning, inflammation and fibrosis for each group is shown below the image. The NAFLD activity score (NAS) for each group was, in average, 0 (zero) for control group with chow diet, 0.8 for the group of mice with Western diet for 4 weeks, 4.4 for the group of mice with Western diet during 10 weeks and 7.8 for the group of mice with Western diet during 24 weeks.

Figure 2.3 shows a boxplot with individual values of the NAS value. The control group, mice fed with Western diet for 4 weeks and two mice fed with Western diet for 10 weeks have no NASH, while the mice fed with Western diet for 24 weeks and four mice fed with Western diet for 10 weeks have NASH.

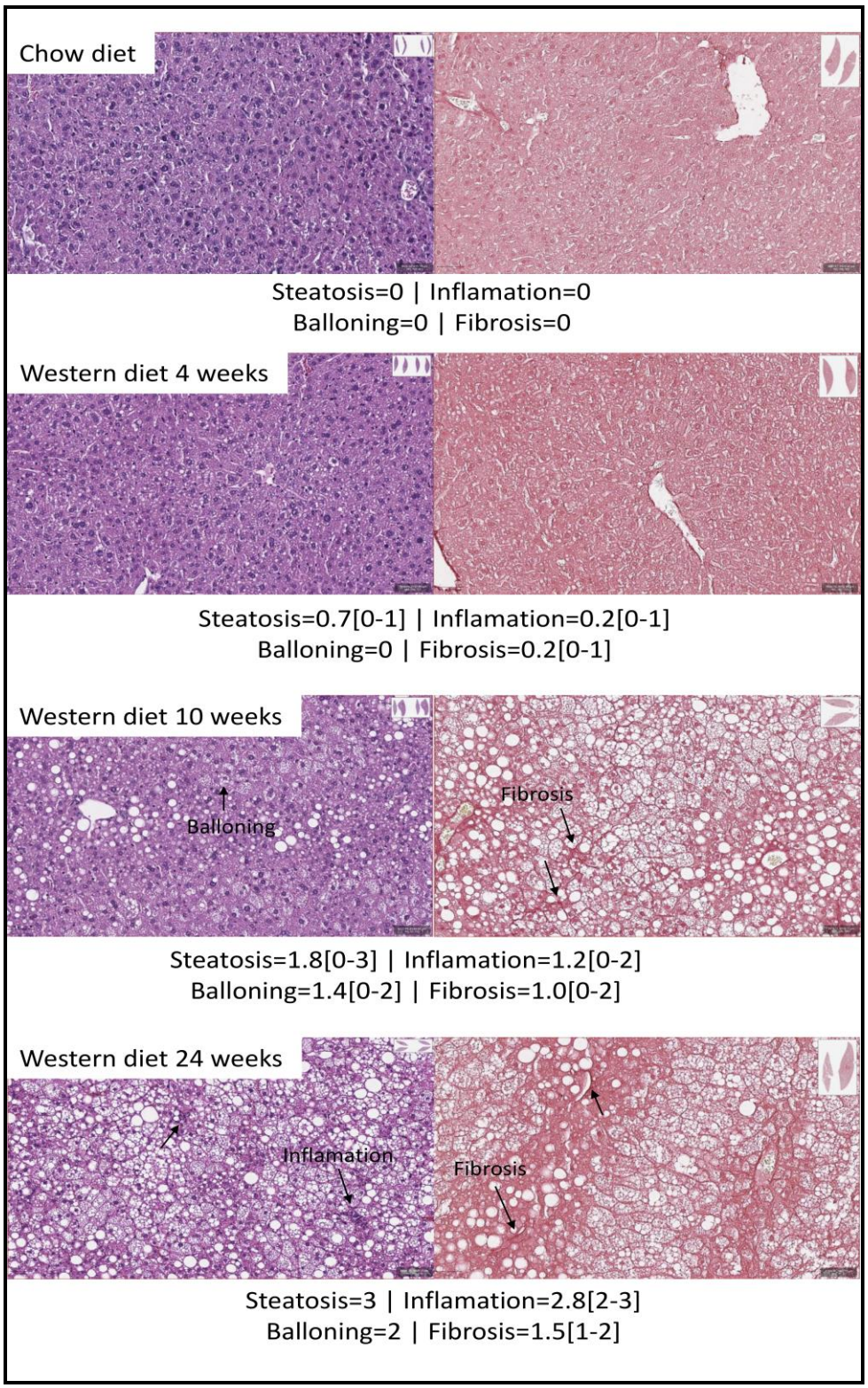

Figure 2.2. Hepatic histology results with hematoxylin/eosin (left) and picrosirius red (right). the average score and the range of steatosis, ballooning, inflammation, and fibrosis for each group is shown below the image.

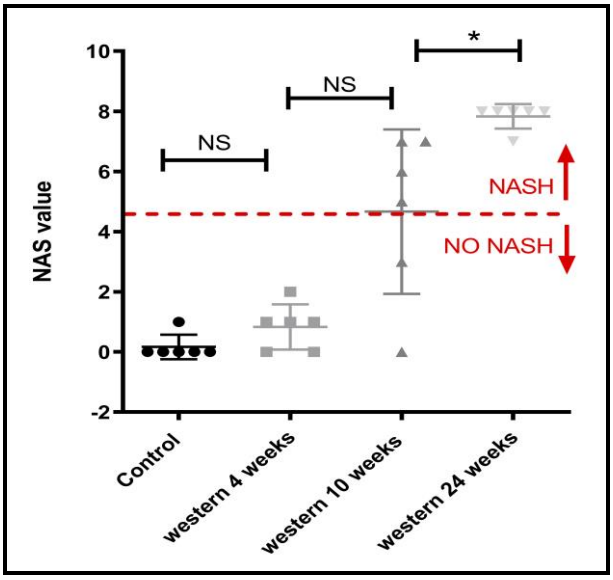

Figure 2.3. Boxplot of NAS value for each mouse individually. NAS value varies between 0 and 8: A value bigger or equal to 5 means that the mouse has NASH.* $p<0.05$ (significant difference between groups) and NS (no significant difference between groups).

2.3.2 Gas Chromatography with Mass Spectrometer

We identified 12 main fatty acids using the CG-MS, however, 5 of them had less than 1% of participation, therefore, we only considered 7 FA for the analysis (C16:0, C18:0, C16:1, C18:1, C18:2, C20:4, C22:6). Two of the FA changed significantly between all the groups (control, 4Weeks-diet, 10Weeks-diet and 24Weeks-diet) corresponding to the progression of NAFLD: C18:1 increased, while C18:2 decreased. Other two FA (C16:1 and, C22:6) changed significantly between 3 of the 4 groups, C16:1 increased, while C22:6 decreased (Figure 2.4). Additionally, by comparing the composition of the fatty acids in two portions of the same liver, we identified a maximum difference of 2.5%, most of them less than 1%.

All the FA can be grouped into three main categories: saturated fatty acids (SFA), monounsaturated fatty acids (MUFA) and polyunsaturated fatty acids (PUFA). The SFA have no double bonds (i.e., C14:0, C15:0, C16:0, C18:0), while the MUFA have one double bond (i.e., C16:1, C18:1) and the PUFA have two or more double bonds (i.e., C18:2, C18:3, C20:3, C20:4, C20:5, C22:6).

Figure 2.5 shows that PUFA liver content decreased with the progression of the disease from 40.5% in control group to 4.5% at 24 weeks (P_{ANOVA}<0.001). In contrast, MUFA liver content increased from 26.8% in control group to 67.8% at 24 weeks (P_{ANOVA} <0.001), while SFA remain constant.

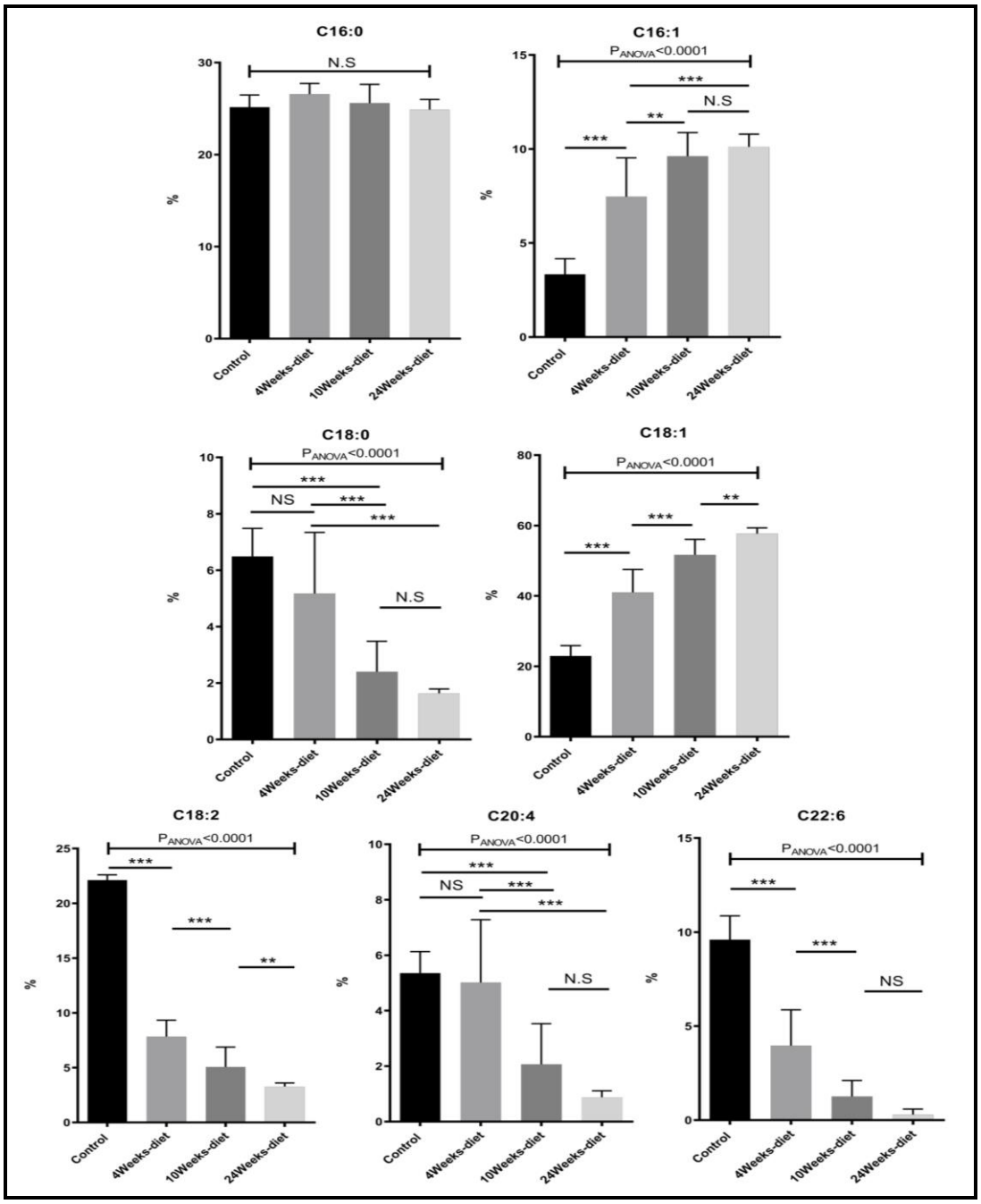

Figure 2.4. Change in Fatty Acids composition measured with GC-MS (mean±SD) for the four different groups of mice (control or chow diet, 4 weeks of Western diet, 10 weeks of Western diet and 24 weeks of Western diet). * p<0.05, ** p<0.01, ***p<0.001 (significant difference between groups) and NS (no significant difference between groups).

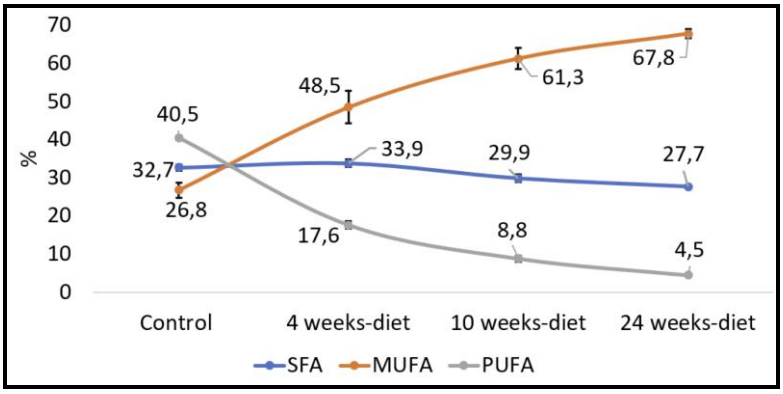

Figure 2.5. The relative contribution of each group of fatty acids: Saturated fatty acids (SFA: C14:0, C15:0, C16:0, C18:0), monounsaturated fatty acids (MUFA, C16:1, C18:1) and Polyunsaturated fatty acids (PUFA, C18:2, C18:3, C20:3, C20:4, C20:5 C22:6).

2.3.3 Magnetic Resonance Spectroscopy

We have identified seven metabolite peaks in the MRS spectra that correspond to the FA and the peak of methyl ester (3.6 ppm). Figure 2.6 shows a visual comparison between a representative spectrum of one control group mouse and the spectrum of a mouse fed Western diet for 24 weeks. Five peaks (terminal methyl, bulk methylene, allylic, diallylic and olefinic) showed significant differences with the progression of the disease (Figure 2.7). However, the terminal methyl group should not change since this peak is present in all FA, with the same quantity of protons. The alfa and beta methylene should be present in all FA with the same number of protons; therefore, we should not expect any significant differences.

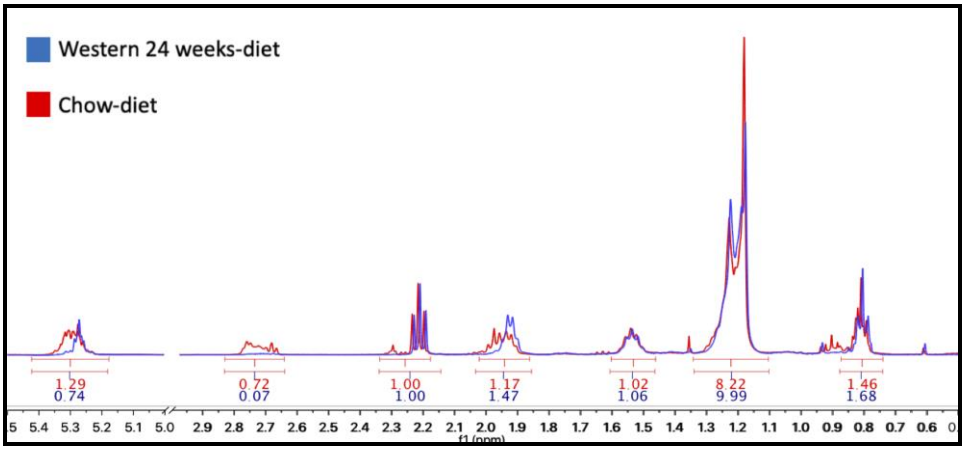

Figure 2.6. Areas under the curve (AUC) calculated with MestreNova V10.0. In red, the results of a control mouse with a chow-diet and in blue, a mouse with a Western diet for 24 weeks.

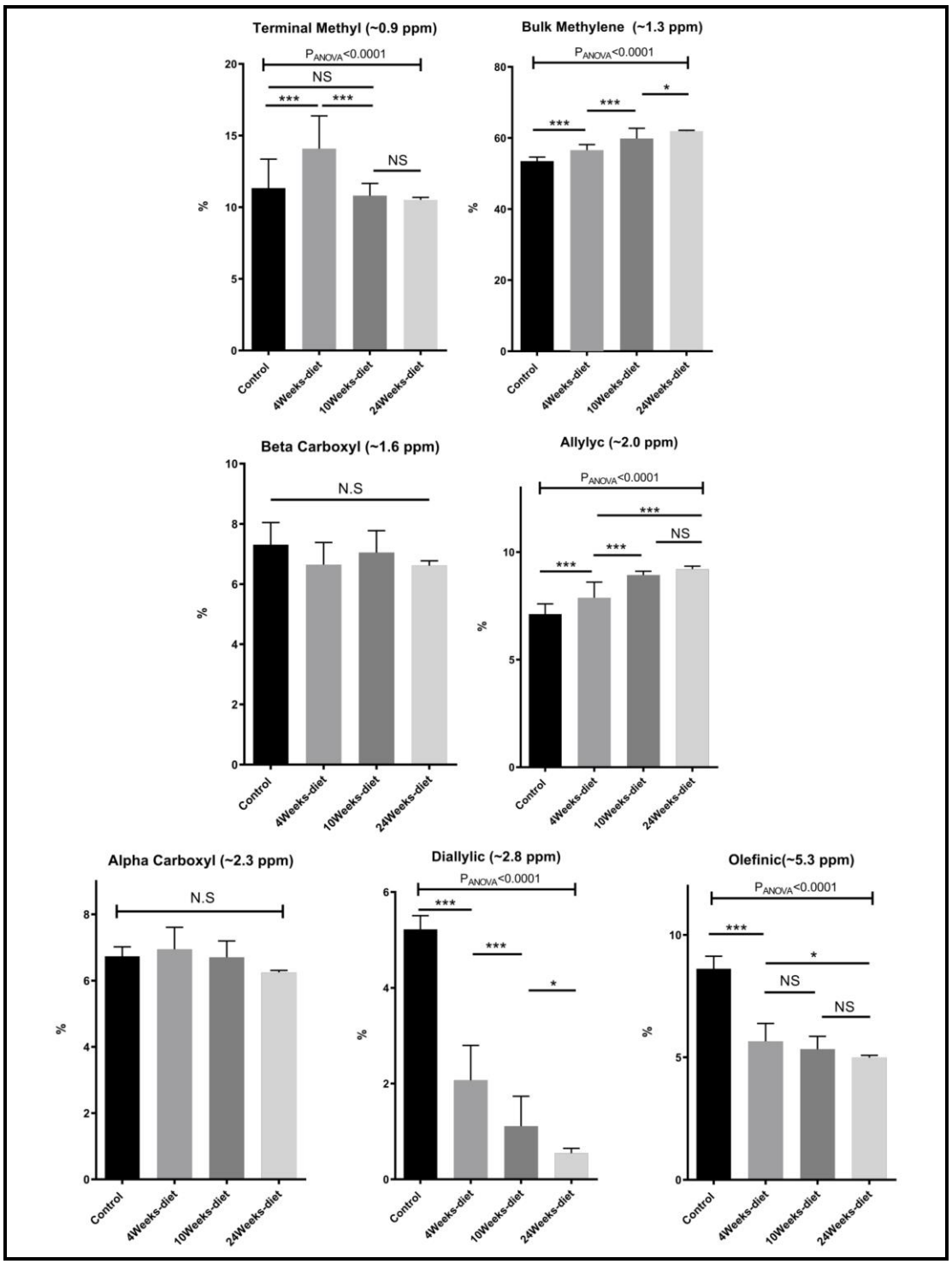

Figure 2.7. Change in the AUC of the 7 peaks measured in the 1H-MRS (mean±SD) for the four different groups of mice (control or chow diet, 4 weeks of Western diet, 10 weeks of Western diet and 24 weeks of Western diet). *p<0.05, **p<0.01, ***p<0.001 (significant differences between groups) and NS (No significant difference between groups).

2.3.4 Principal Component Analysis

The principal components for the FA composition measured with GC-MS and metabolites identified in the ^{1}H-MRS were computed separately; and the data projected onto the space generated by their corresponding first two principal components (Figure 2.8a,b). In this 2-dimensional representation it is possible to identify changes in the GC-MS measurements as the time of diet intervention increases and the disease progresses (Figure 2.8a). In particular, the control group and the mice fed for 24 weeks are well-separated. This behavior is replicated for the ^{1}H-MRS measurements (Figure 2.8b) indicating the potential for ^{1}H-MRS to be used both as a biomarker for the progression of the disease and as a surrogate for GC-MS.

The three groups that can be visually identified show a rough correlation with the number of weeks each mouse has been fed (Figure 2.8 a,b). Interestingly, the group of mice fed for 10 weeks has been split in two, with some of them grouped with mice fed for 4 weeks, and the rest grouped with mice fed for 24 weeks. Those grouped with the mice fed for 4 weeks are those with no NASH whereas those grouped with the mice fed for 24 weeks are precisely those that have NASH (Figure 2.3).

We used agglomerative hierarchical clustering to group both the GC-MS and ^{1}H-MRS data (Figure 2.8c,d). Interestly, the clusters obtained correspond to three stages of NAFLD: the first one with a low NAS value, normal; the second one, with an intermedium NAS value, low to medium steatosis; and the third one with high NAS value with inflammation and early stages of fibrosis. The dendogram of the agglomerative Hierarchical Clustering can be appreciate in the Figure 2.9 and the black arrow shows the cut-point, grouping the samples in three clusters with 100% of agreement: It means that all the mice found in the one group belonging to GC-MS are the same mice found in MRS.

Furthermore, the mouse whose result is at the top of the GC-MS graph (Figure 2.8a) was grouped as a control mouse, even though it was fed with Western diet for 4

weeks. However, its NAS value was 0. Figure 2.10 shows the mean of NAS value for each the cluster identified (control, No NASH, NASH).

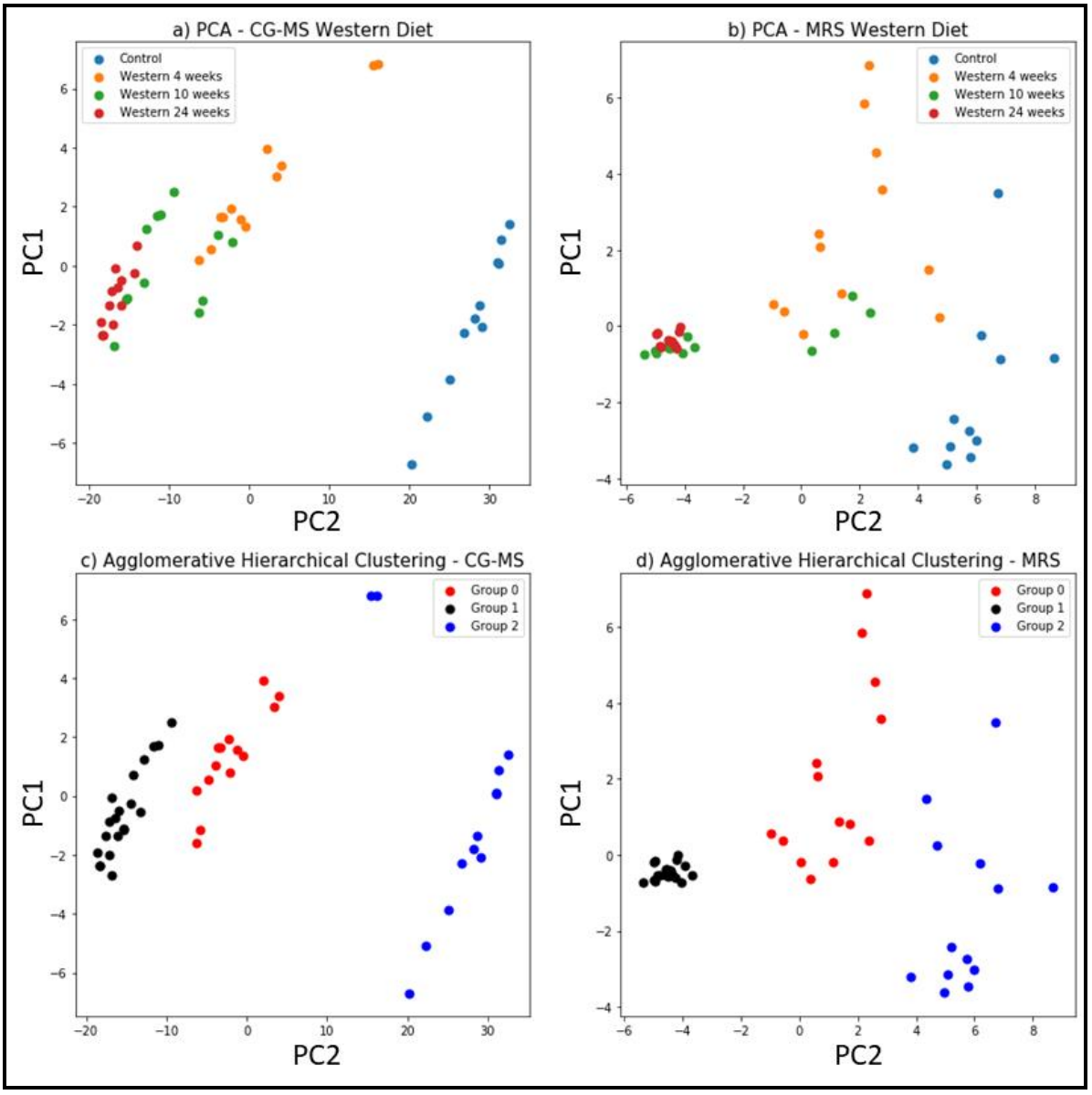

Figure 2.8. Principal component analysis of GC-MS results (a) and MRS results (b) for all the groups of mice (control, 4 weeks Western diet, 10 weeks Western diet, and 24 weeks Western diet). Agglomerative Hierarchical Clustering method to cluster the data of GC-MS (c) and MRS (d). X-axis id the principal component 1 and y-axis is the principal component 2.

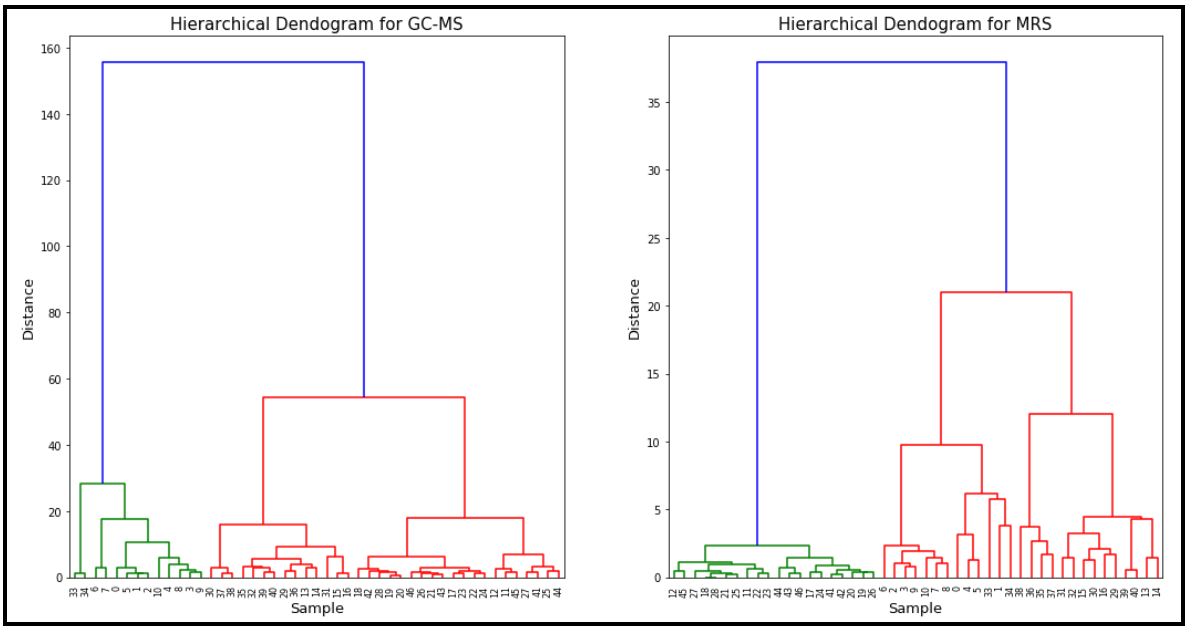

Figure 2.9. Dendogram of the agglomerative Hierarchical Clustering obtained by the results of GC-MS (on the left) and MRS (on the right). The x-axis are the samples and y-axis are the distance. The black arrow shows the cut-point.

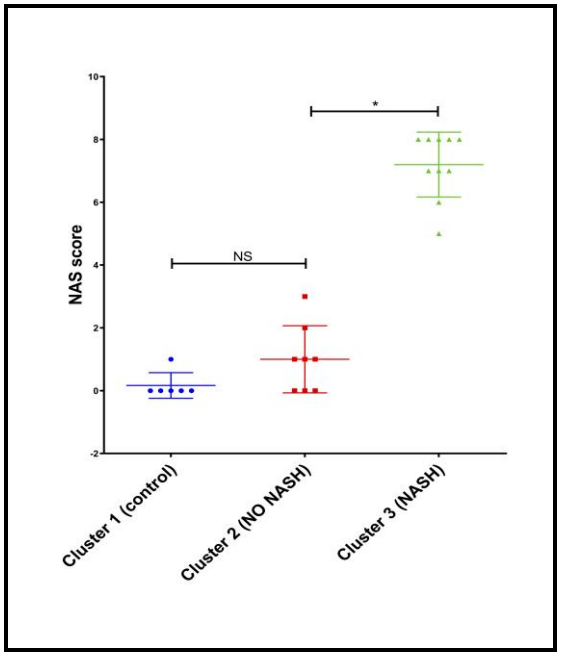

Figure 2.10. NAS value for each cluster found by PCA with the data from GC-MS and MRS. * $p<0.05$ (significant difference between groups) and NS (no significant difference between groups).

2.4 Discussion

We have analysed the effects of a diet intervention with a fast food-like model (*i.e.*, Western diet) in mice for 24 weeks. During the progression of the disease, the mice consecutively develop steatosis, steatohepatitis, and liver fibrosis, with a progressive increase in the NAS value. Simultaneously, Western diet produced numerous changes in liver fatty acids composition, which could provide new evidence to understand the progression of the disease and identify biomarkers to predict the progression of steatosis and NASH.

GC-MS analysis showed that the fat in the liver is composed of, at least, 12 different fatty acids, which have different evolution during the NAFLD progression. Besides that, the analysis identifies a pattern of fatty acids composition during NAFLD progression: although the total amount of fatty acids increased during the NAFLD progression, not all the fatty acids progressed in the same way. The PUFA decreased, while the MUFA increased and the SFA remained the same during the progression of the disease. Similar results were found by Levant et al. (2013) in mice with a high-fat diet for 8 weeks. The decrease in the PUFA can be explained since the arachidonic (C20:4); eicosapentaenoic acid (20:5) and docosahexaenoic acids (C22:6) are precursors for a variety of anti- and pro-inflammatory mediators (Bazan, 2005), (Bannenberg et al, 2007).

MRS analysis found all the seven peaks related to fatty acids. The diallylic peak (2.8 ppm), corresponding to FA with two or more double bonds, also decreased in good agreement with the PUFA results found by CG-MS. The olefinic (5.3ppm), allylic (2.0 ppm) and bulk methylene (1.3 ppm) peaks are somehow related to this change in PUFA and MUFA, because they are related to double bonds.

As mentioned by Leporq et al. (2014), who used only theoretical values calculated from oil mass composition for validation, one of the limitations of their work was not to have the gas chromatography analysis as gold standard to characterize those FA (Leporq et al, 2014). Opposite to this, our study overcomes this limitation with the GC-MS analysis.

Our results, as evidenced by PCA, showed that the liver fatty acid composition changes as NAFLD progresses. In addition, by using agglomerative hierarchical clustering it was possible to identify the 3 most relevant clinical groups: normal, steatosis and NASH. In essence, the NAS value of the entire population was reproduced by clustering the GC-MS data in three groups. In addition, applying the same analysis to the ^{1}H-MRS data shows it is possible to identify the same 3 groups using ex-vivo MRS, which provide some evidence that the proposed methodology could be used in-vivo and non-invasive, however further studies has to be done to prove this hypothesis.

Some limitations of our studies are related to the possibility that our results may vary if the mice were fed with different diets, although we have used the diet most like human diet (Tetri et al, 2008), (Longato, 2013). However, this limitation might explain differences in the NAFLD progression among patients, in which some of them evolve to NASH and cirrhosis, whereas others remain in the early stages of NAFLD for a long time.

Additionally, the MRS acquisition was performed only over the extracted liver fatty acids, so that it is now necessary to validate our results with in-vivo whole liver MRS acquisition. The transition to an in-vivo measurement has some challenges since it may account with a series of extra parameters like respiratory and cardiac motion, presence of water component, the correlation between acquisition time, NSA, voxel size and SNR to assure the comfort of the patient, but also the spectra quality.

Preliminary results showed that it would be possible to identify the same 7 peaks in human and mice livers in-vivo at 7.0T (Fillmer et al, 2019) and 9.4T (Xavier et al, 2019), respectively (Figure 2.11). Although the 7.0 T is not available for clinical use yet, research could be made in this equipment by benefitting from its good spectral resolution to validate the method. Additionally, the peak in 3.2 ppm is the choline peak and the mouse spectrum is from a mouse with a diet deficient in choline, therefore this mouse presents no signal at peak in 3.2 ppm.

To conclude, our study compares different stages of the NAFLD disease induced by a Western diet. The differences in the FA composition found by GC-MS, which is

also reflected in the MR spectrum, could have clinical potential for monitoring NAFLD progression from steatosis to NASH in a non-invasive way.

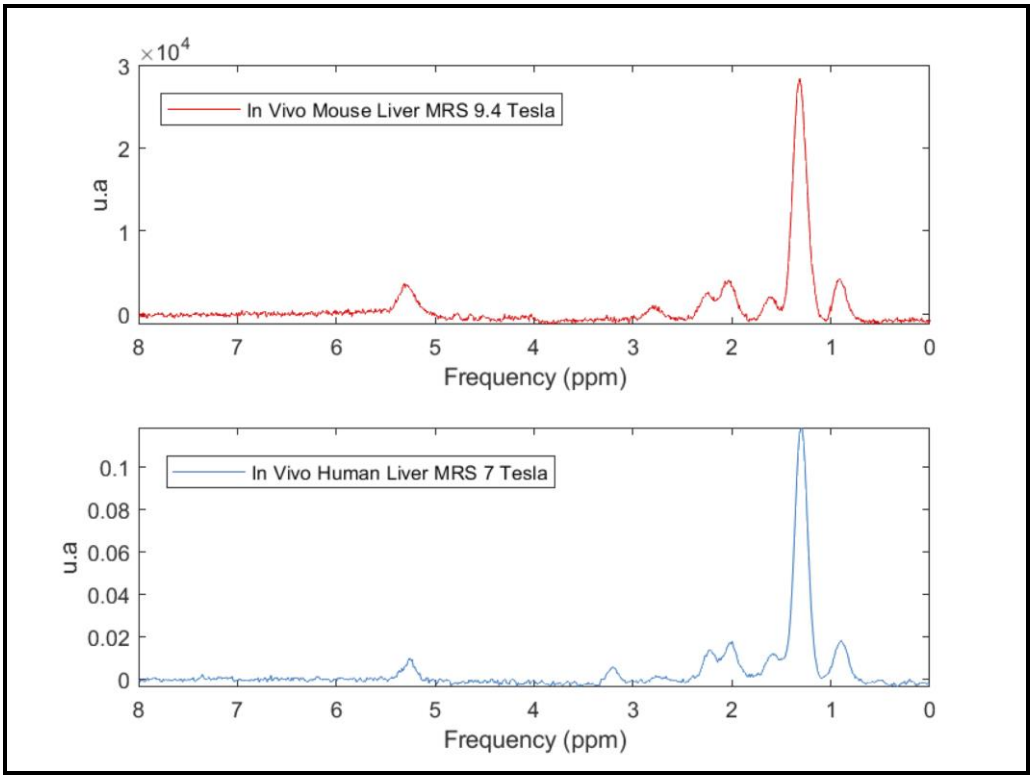

Figure 2.11. In-vivo MR spectra from a 9.4 Tesla in a mouse (red) and 7 Tesla in human (blue) showing that it is possible to identify all the seven peaks correspondent to the fat spectrum in the liver.

3. EX-VIVO AND IN-VIVO STUDY IN MICE MODEL FED WITH CDAA DIET

This chapter is based on the following submitted article and was performed in collaboration with School of Biomedical Engineering and Imaging Sciences, St Thomas' Hospital, Kings College London, London, UK

Xavier, A., Zacconi, F. C., Santana-Romo, F., Eykyn, T., Lavin-Plaza, B., Phinikaridou, A., Botnar, R., Uribe, S., Oyarzún, J.E., Cabrera, D., Arrese, M., Andia. M.E. (2020). Intrahepatocyte fatty acids characterization in a mice model during NASH progression using *in vivo* and *ex vivo* magnetic resonance spectroscopy**.** [under review]

3.1 Introduction

Non-alcoholic fatty liver disease (NAFLD) consists of a group of liver disorders starting with steatosis, and progressing to steatohepatitis (NASH), fibrosis, and finally, a small percentage progress to form cirrhosis and liver failure. The current gold standard used to confirm and stage NAFLD is invasive liver biopsy, which is of high risk for patients (Friedman et al, 2018). Diagnosis of NAFLD is usually based on an estimation of the total amount of hepatic fat infiltration and does not show a good correlation with clinical progression (McClain et al, 2007). Total fat accumulation does not consider differences in lipid composition such as presence of different fatty acids (FA), which has been proposed as an alternative method to discriminate these diseases (Puri et al, 2007), (Araya et al, 2004), (Xavier et al, 2019b). Understanding the evolution of FA composition during disease progression would aid stratification, prognosis, and evaluation of treatment response as well as leading to a better understanding of the evolution of this disease.

FA composition can be measured using ex-vivo Magnetic Resonance Spectroscopy (MRS) or mass spectrometry-based approaches of extracted tissue samples, or non-invasively using in-vivo volume localized MR spectroscopic imaging techniques (Hamilton et al, 2011), (Longo et al, 1995), (Johnson et al, 2008). Ex-vivo MRS provides metabolic information with higher spectral resolution and sensitivity than in-vivo MRS (Claridge, 2016). It also allows to compare results with other analytical methods like gas

chromatography with mass spectrometry (GC-MS), which is the gold standard to quantify FA composition, and histology, which is the gold standard to classify the stage of NAFLD disease. In-vivo MRS is commonly used to assess metabolic information either in clinical or preclinical studies, and a big advantage is that it allows longitudinal assessment of the same subject during the disease's progression/regression.

There are a number of murine models to study NAFLD (Machado et al, 2015), (Hariri & Thibault, 2010), (Sanches et al, 2015), (Lau et al, 2017), (Van Heck et al, 2017), (Hebbard et al, 2011), including dietary models and genetic models. Within the former, diets that are rich in fat and mimic the human diet, generate metabolic disorders and increased accumulation of liver fat (eg: high-fat diet and Western diet). The drawback to this model is that animals take a long time to develop steatosis and NASH, and a low proportion of them show progression to cirrhosis. There are also diets which generate inflammation and liver injury such as CDAA (*choline-deficient*, l-amino acid-defined) (Van Heck et al, 2017) and MCD (methionine and choline-deficient) (Machado et al, 2015) diets. The MCD diet has disadvantages when compared to others since mice start to lose weight, have reduced levels of insulin and glucose and the phenotype does not recapitulate what is observed in humans (Sanches et al, 2015). On the other hand, CDAA is an aggressive diet and animals develop liver inflammation as early as three weeks (Hansen et al, 2017), allowing the study of the longitudinal evolution at more time points during NASH stages and fibrosis. This model does not accurately represent the human progression from NAFLD to NASH but allows to study the progression from NASH to cirrhosis.

In previous work (Xavier et al, 2019b), we studied the progression of NAFLD from steatosis to steatohepatitis in mice fed Western diet for 24 weeks, using MRS of ex-vivo tissue samples. We found a decrease in polyunsaturated fatty acids (PUFA) and an increase of monosaturated fatty acids (MUFA) during progression of the disease. The reduction in PUFA was associated with a rise in liver inflammation (Bazan, 2005), (Bannenberg et al, 2007). Additionally, employing the MRS data, the disease could be classified using principal component analysis (PCA) into three categories: normal, steatosis, and NASH, where it was possible to correctly classify the groups according to the gold standards methods (Xavier et al, 2019b). However, a major limitation of this study was the use of only one type of diet, and MRS analysis was only performed in ex-vivo samples.

To our knowledge, there are no studies of liver FA composition and evolution during liver injury caused by CDAA diet. This study aims to compare liver FA composition in the progression of NAFLD with a mouse model fed CDAA diet during the progression of NASH. We used a combination of both ex-vivo and in-vivo MRS techniques at 9.4T to perform a complete characterization of liver lipid changes during a CDAA diet intervention. These techniques have not been performed together before for this purpose.

3.2 Subjects and methods

Ex-vivo experiments were carried out at Pontificia Universidad Católica de Chile, Santiago, Chile. All experiments were approved by the Scientific Ethics Committee for the care of animals and the environment (Comité de ética y bienestar Animal, Escuela de Medicina, Pontificia Universidad Católica de Chile [CEBA] resolution #14-048). In-vivo experiments were carried out at King`s College London, London, UK. All animal experiments were conducted in accordance with the Home Office Animals (Scientific procedures) Act, UK, 1986 and were approved by the King's College London ethical review committee.

3.2.1 Animal diet

For the ex-vivo study, mice (C57BL/6) were fed with a CDAA diet (#518753, Dyets Inc. Bethlehem, PA, composition: 11.68% cornstarch, 11.68% dextrin, 47.49% sucrose, 5.84% cellulose, 5.84% corn oil, 11.68% Primex, 4.09% salt mix, 0.5% sodium bicarbonate, 1.17% vitamin mix, 0% choline, 0.04% ferric citrate) for four weeks (n=6) and another group for ten weeks (n=6). We also fed a control group (n=6) with a Chow diet (500l*, Labdiet, Missouri, USA).

For the in-vivo study, we fed four mice for ten weeks, acquiring images/spectra during weeks 4, 6, 8, and 10 and a control group (n=4) with a Chow diet.

3.2.2 Ex-vivo study

At the end of the diet intervention, mice were anesthetized with ketamine/xylazine, and the livers were harvested (Cabrera et al, 2017). A portion of the liver was used for histology. The remaining liver was divided into two portions for independent analysis. Intracellular FA were extracted using a protocol adapted from Folch et al.(1957), followed by esterification to obtain more stable fatty acid methyl esters (FAME). It is important to note that the quantity of FA is the same as FAME. Finally, FAME were analysed using a 9.4T MRS or GC-MS. From previous studies (Xavier et al, 2019a) we found that 300 mg of the liver from healthy mice was sufficient to obtain 5 mg of FAME, which is the minimum amount of sample needed to perform a MRS (400MHz) with good SNR while only 2 mg of FAME is required for GC-MS.

FAME Extraction

Fatty acids were extracted in the form of methyl esters. Briefly, the liver was weighted and homogenized for 5 minutes, under an ice bath, with a known amount of $CHCl_3$/MeOH (2:1), NaCl, CH_3COOH and C19 (as standard) and the organic phase was extracted. The solvent was removed by evaporation by blowing nitrogen gas. Once completely dry, the final mass of FA extracted from the initial liver mass was obtained.

The esterification process was carried out by adding 1 mL of 10% acetyl chloride in anhydrous methanol, and 0.5 mL of dry toluene as a solvent and brought up to 55 degrees Celsius overnight. The next day, each sample was neutralized with approximately 7 mL of 6% sodium bicarbonate, immersed for 5 seconds in a sonication bath to separate it from the organic phase.

2 mL of n-hexane (HPLC grade) was added for the final extraction of the FAME, to which, after a centrifugation process to remove residual water, the solvent was displaced with nitrogen gas and the final methyl esters mass was obtained.

Histology

Liver sections were fixed in 10% formalin, embedded in paraffin and then 5 mm tissue sections were stained with hematoxylin/eosin, oil red, and Picrosirius Red, as described previously (Cabrera et al, 2017). Whole slide imaging was performed using an Aperio Digital Pathology Slide Scanner (Leica Biosystems), allowing us to study the entire left lateral lobe. Histopathological analysis was performed by a blinded pathologist starting from three full cross-sectional slides obtained from distal, medial, and proximal regions derived from the left lateral lobe. The blinded trained pathologist utilized the NAFLD Activity Score (NAS) proposed by Kleiner et al.(2005) The score for steatoses varies between 0 and 3; for ballooning between 0 and 2; for inflammation between 0 and 3, and for fibrosis between 0 and 4. NAS is defined as the sum of steatosis, ballooning, and inflammation with a value between 0 and 8. A NAS score less than 3 means no NASH, while a score higher than 4 means NASH. Scores of 3 or 4 are indeterminate.

GC-MS

FAME were analysed using GC-MS (PerkinElmer, Clarus 680) equipped with HP-Innowax capillary column (length 25 meters, 0.2 mm internal diameter, 0.2 mm film). The injector temperature was kept at 220ºC, and the oven ramp was 150ºC x 1 min, changed to 200ºC at a 15ºC/min rate and it was maintained for 5 min, and then the temperature was increased from 200ºC to 260ºC at a 12ºC/min rate. Sample injection was in split mode (1:20) with Helium as the carrier gas with the flow of 1ml/min. Electron impact ionization mode of mass detector was set with ionization potential of 70eV. Data register was in SCAN mode, and peak integration was obtained by the TurboMass Training 2016 PRO software. FAME were identified by comparing retention times to known standards and by matching them with the mass spectra from NIST library (National Institute of Standards and Technology, USA). The mass of each FAME (in µg) was calculated according to the integration area of the corresponding peak, and the relation with the integration area of the internal standard (C19:0). Fatty acids composition was defined as the percentage of individual fatty acids in respect of its total.

MRS

^{1}H-MRS spectra of the FAME were obtained using a Bruker Avance spectrometer operating at 9.4 T with the acquisition protocol Zg30 (30 degrees excitation pulse). A known mass of FAME from each sample was dissolved in 0.7 ml of $CDCl_3$ containing tetramethylsilane (TMS) as an internal reference. The sample was introduced into a 5 mm diameter tube. Spectra were acquired with Topspin V3.0 at 298K and a spectral width of 8012.8 Hz, relaxation delay 1 s, number of scans 16, acquisition time 2.045 s, flip angle 30° (to avoid T1 relaxation effects) and total acquisition time 48.7 s.

3.2.3 In-vivo study

MRS

Mice were anesthetized with 1% isoflurane, and their temperature was monitored continuously. Liver MRS was obtained in a 9.4 T vertical magnet (Bruker UltraShield 400WB Plus) with a surface coil (Bruker BioSpin MRI GmbH). Single voxel spectroscopy was acquired using a stimulated echo acquisition mode (STEAM) with and without water suppression. Water suppression employed variable pulse powers and optimized relaxation delays (VAPOR). First, a fast low angle shot (FLASH) localizer image was performed (2D, TR = 30ms, TE = 1.8ms, NSA = 2, Flip angle = 30) with B_0 shimming, followed by a fast imaging with steady state precession (FISP) localizer (2D, TR = 4ms, TE = 1.8ms, NSA = 3, Flip angle = 7, number of images = 30). A minimum of 2 voxels were selected for each mouse, and for each voxel, localized shimming (B_0) was performed. The acquisition parameters for the STEAM were TR/TM/TE= 2500/10/3ms, BW=5500 Hz, Nº points=2048, NSA=32, Voxel = 2x2x2 mm^2, total scan time = 1m20s (Figure 3.1). After the study, mice were euthanized by an overdose of anesthesia.

Spectra were fitted with the Advanced Method for Accurate, Robust and Efficient Spectral fitting (AMARES) in the jMRUI software package (Stefan et al, 2009), (Vanhamme et al, 1997). The fatty acids peaks considered were: terminal methyl protons ($–CH_3$, approximately at 0.9 ppm); bulk methylene protons ($(–CH_2–)_n$, approximately at 1.3 ppm);

β-methylene protons (-COO–CH_2–CH_2–, approximately at 1.6ppm); allylic protons (–CH_2–CH=CH-CH_2, approximately at 2.0 ppm) α-methylene protons (-COO–CH_2–, approximately at 2.2 ppm); diallylic protons (-CH=CH–CH_2–CH=CH-, approximately at 2.8 ppm) and olefinic internal protons (–CH=CH–, approximately at 5.3 ppm).

Total lipid content in the liver was calculated as L/(L + W) * 100%, where W represents the amplitude of the water signal and L the total amplitude of the lipid signals. Signals were corrected for T_1 and T_2 relaxation time.

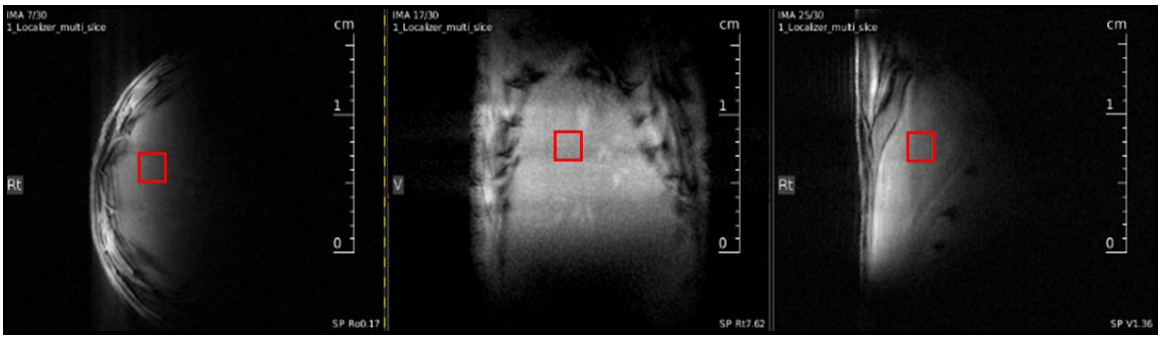

Figure 3.1. In-vivo voxel positioning to perform the STEAM sequence with TR/TM/TE= 2500/10/3ms, BW=5500 Hz, Nº points=2048, NSA=32, Voxel = 2x2x2 mm^2, total scan time = 1m20s.

3.2.4 Statistical analysis

All statistical analyses were performed using Prism 6 (GraphPad Software Inc, La Jolla, CA). The data have normal distribution as confirmed by Shapiro-Wilk test. All graphs were plotted as mean, standard deviation, or boxplot. To compare among three or more groups, the ANOVA test was performed followed by a Bonferroni post-hoc test. A P-value < 0.05 was considered to indicate statistical significance.

3.3 Results

3.3.1 Ex-vivo study

Figure 3.2A shows body weight, liver weight, and the total liver FAME content (mass of FAME/total liver sample, %) for each group (control, 4 weeks of CDAA diet, and 10

weeks of CDAA diet). By comparing the percentage of FAME in two portions of the same liver (that were analysed independently before averaging), we identified an average difference of 2.3%.

Figure 3.2B shows representative histology of liver sections for control group (I) and 4 weeks of CDAA diet (II) with hematoxylin/eosin, where one can visualise macrovesicular steatosis, ballooning and inflammation; and 10 weeks of CDAA diet (III) with Picrosirius Red, where one can also visualise fibrosis. The NAS value confirmed the progression of the disease (Figure 3.2C), and the liver doubled in size when comparing the liver from the control group with a mouse with NASH liver, fed with CDAA diet for only 4 weeks (Figure 3.2D).

Figure 3.3A shows the FAME spectrum from a mouse belonging to control group, a mouse belonging to the group fed with CDAA diet for 4 weeks and another one from the group fed with CDAA diet for 10 weeks. Differences in the FA composition between control group and CDAA-diet group can be appreciated, notably at 2.8 ppm (diallyc peak) and 5.3 ppm (olefinic peak).

From the MRS spectra, we found seven peaks correspondent to lipids, 3 of them are similar in all FA (0.9 ppm; 1.6 ppm; 2.2 ppm); therefore, they present no significant differences (Xavier et al, 2019b). The other four peaks showed significant differences between the control group and the 4 weeks of diet group but then no further significant differences between 4 and 10 weeks of diet groups (Figure 3.3B).

The results from GC-MS are in according to the results obtained with MRS, so it also presented significant differences between the control group and the 4 weeks of diet group but no significant differences between 4 and 10 weeks diet groups (Figure 3.3C).

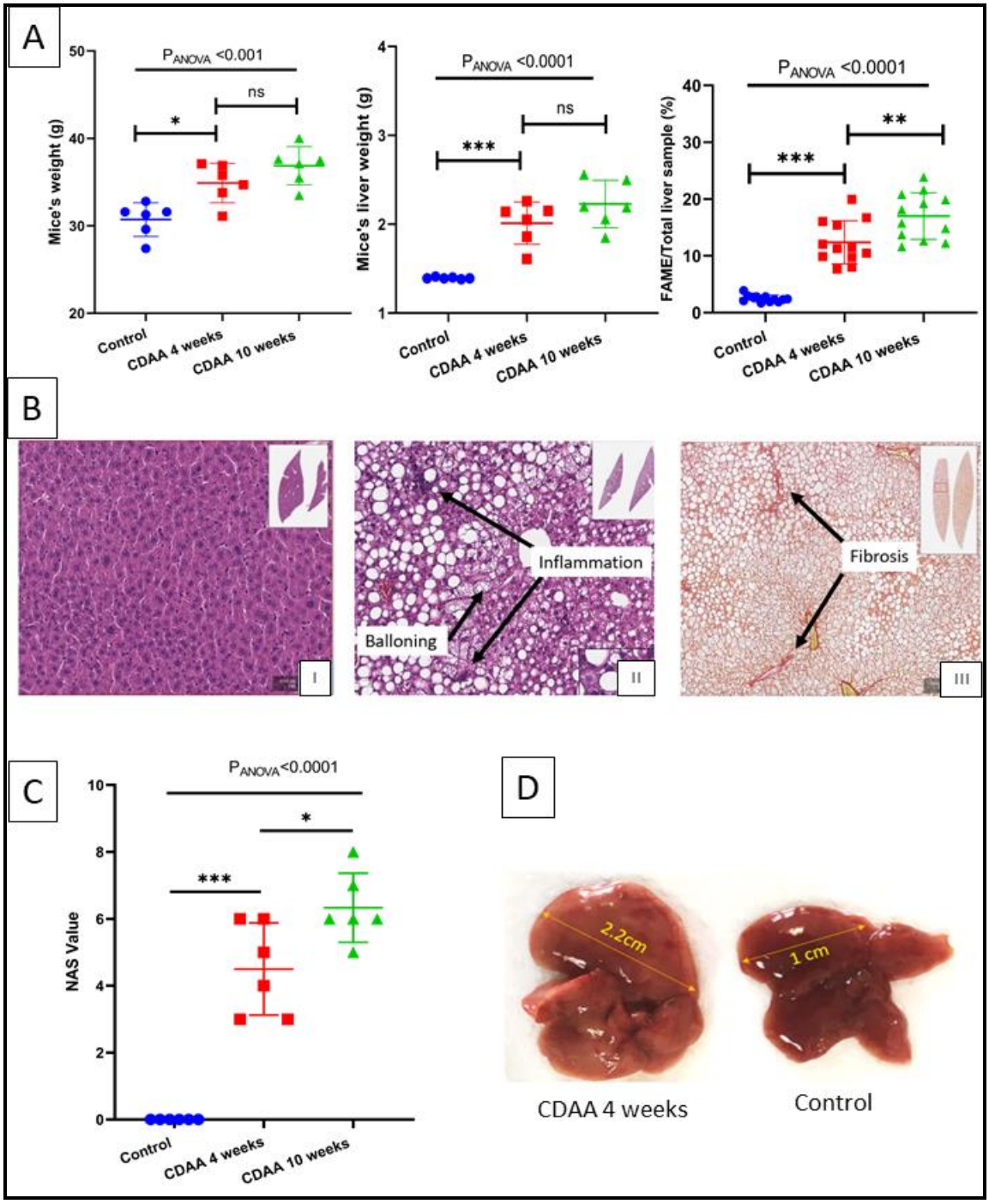

Figure 3.2. (A) Mice´s weight, liver weight and percentage fatty acids in the liver for each group. (B) Liver histology sections of control group (I) and 4 weeks-diet (II) with hematoxylin/eosin, where macrovesicular steatosis, ballooning and inflammation can be visualised; and 10 weeks-diet (III) with Picrosirius Red, where fibrosis can be visualised. (C) Boxplot of NAS value for each mouse individually. *p < 0.05, **p < 0.01, ***p < 0.001 (significant differences between groups) and (D) the liver size comparing 4 weeks CDAA diet and the control group with chow diet.

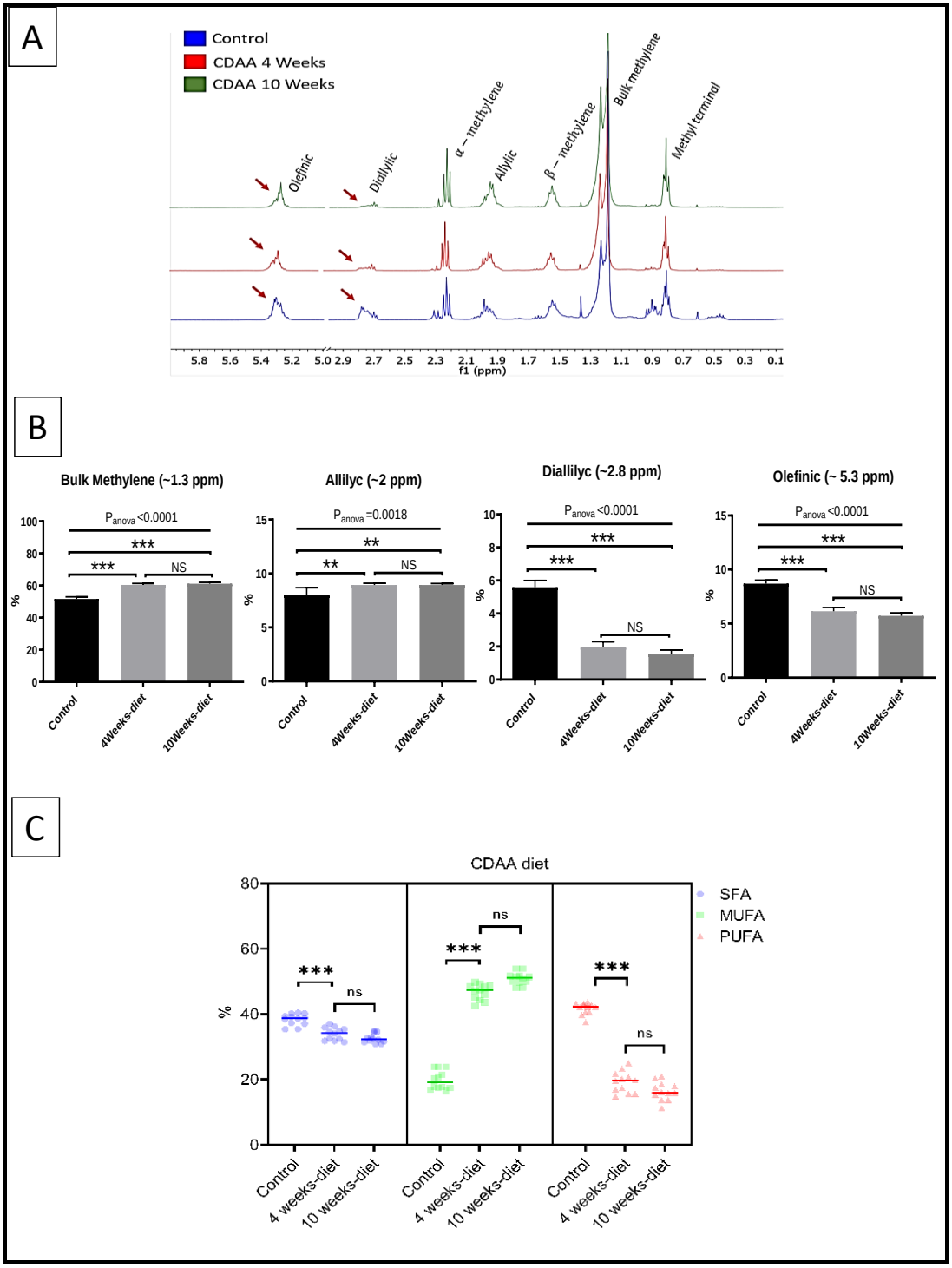

Figure 3.3. (A) MRS spectra from control, mice fed with CDAA for 4 weeks and 10 weeks. (B) MRS data: change in the AUC of the 4 peaks measured in the 1H-MRS (mean ± SD). *p < 0.05, **p < 0.01, ***p < 0.001 (significant differences between groups). (C) The relative contribution of each group of fatty acids: Saturated fatty acids (SFA: C14:0, C15:0, C16:0, C18:0), monounsaturated fatty acids (MUFA, C16:1, C18:1) and Polyunsaturated fatty acids (PUFA, C18:2, C18:3, C20:3, C20:4, C20:5 C22:6) for mice fed with CDAA diet *p < 0.05, **p < 0.01, ***p < 0.001 (significant differences between groups), ns means no significant difference.

3.3.2 In-vivo study

Figure 3.4A shows the mice's weight (on the left) and the lipid content (on the right) for each mouse individually. Lipid content increased from 1.1±0.2% (Control group) to 35.0±4.3% (8 weeks of CDAA diet), $p<0.05$, and then remained the same from 8 weeks to 10 weeks-diet 34.0±4.8, $p>0.05$ although three mice had a decrease in the quantity of fat in the liver, possibly showing signs of fibrosis. Over the same period the weight of the mice increased. The results of control group were the average of the mice with a Chow diet.

From the MRS results, we found seven peaks corresponding to lipids, three of them showed no significant differences (0.9 ppm; 1.6 ppm; 2.2 ppm). Four peaks showed significant differences between the control group and CDAA-diet group. The diallylic peak showed a small but significant difference between 4 weeks and 8 weeks, and between 4 and 10 weeks of CDAA diet (Figure 3.4B) and the other peaks (bulk methylene, allilyc and olefinic) showed no significant differences from week 4 of diet to 10 weeks of diet.

3.3.3 Differences between the in-vivo and ex-vivo MRS

A spectral comparison showed good agreement between in-vivo and ex-vivo results (Figure 3.5A). In the in-vivo spectrum, we can see all the seven peaks corresponding to the fatty acids plus the peaks corresponding to residual water (at 4.7 ppm) and glycerol (around 4.2 ppm), which are eliminated in the extraction process made for the ex-vivo analysis. Figure 3.5B shows the comparison of the metabolites (value in percentage) in-vivo and ex-vivo obtained from the mice liver that were submitted to a CDAA diet for 4 weeks and 10 weeks. We can see significant differences when comparing the in-vivo and ex-vivo results from the diallylic and allylic peak; however, these differences are around 1%.

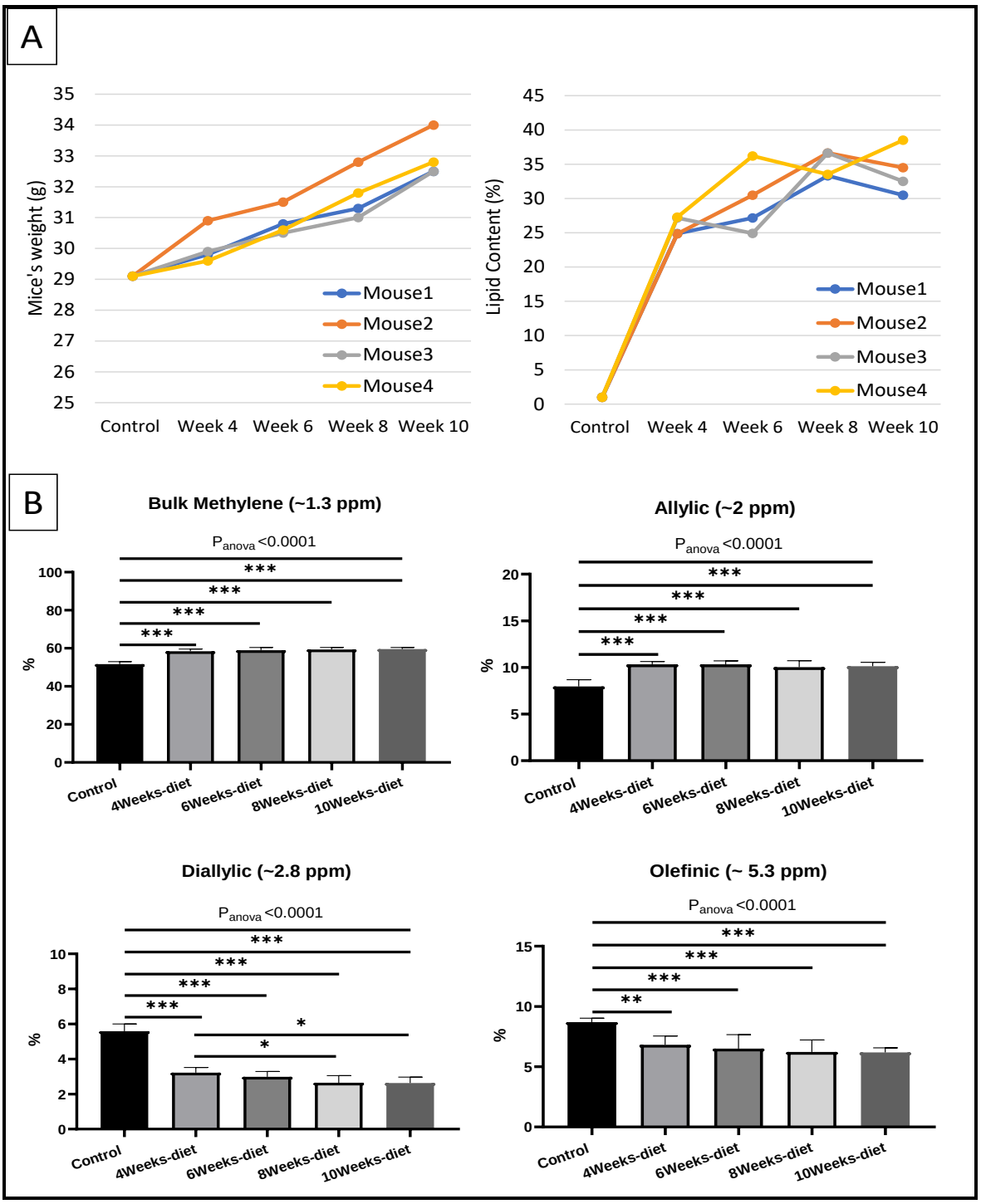

Figure 3.4. (A) In-vivo results: Mice's weight (on the right) and the lipid content (on the left) for each mouse individually. Total lipid content (%) in the liver was calculated as L/(L + W) * 100, where W represents the amplitude of the water signal and L the total amplitude of the lipid signals. (B) In-vivo results from MRS.

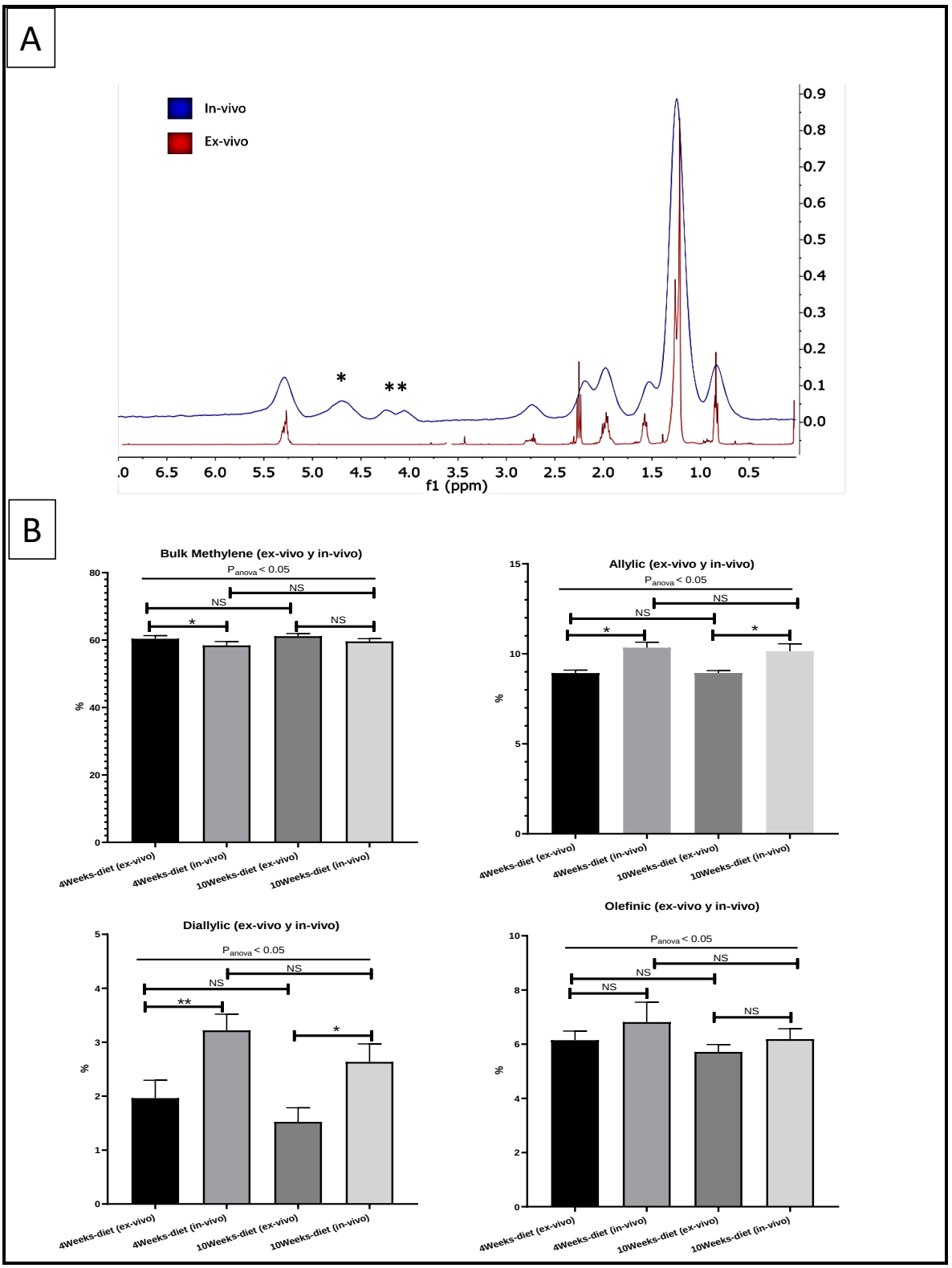

Figure 3.5. (A) Graph showing the MRS in-vivo (blue) and ex-vivo (red). Residual water (*, at 4.7 ppm) and glycerol (**, around 4.2 ppm), are eliminated in the extraction process made for the ex-vivo analysis. (B) MRS results comparing metabolites in-vivo with ex-vivo.

3.4 Discussion

We have analysed the liver fatty acids composition in WT mice fed for 10 weeks on a CDAA diet. The lipid profile was followed longitudinally in-vivo using MRS and ex-vivo using a combination of MRS, GC-MS, and histology. CDAA is very aggressive diet, and the mice already developed NASH after four weeks, as demonstrated by the NAS value. The lipid content increased with disease progression until 8 weeks of diet, but from 8 weeks to 10 weeks, the lipid content started to decrease in some mice, showing some signs of liver fibrosis. An increase in the NAS value confirmed the progression of the disease. Disease progression also produced changes in fatty acid composition following 4 and 10 weeks of CDAA diet compared to control group, although there was no difference between 4 and 10 weeks of CDAA diet.

Ex-vivo MRS analysis displayed seven peaks related to fatty acids. The bulk methylene (1.3 ppm) and allylic (2.0 ppm) peaks increased from control mice group to 4 weeks of CDAA diet group while the diallylic (2.8 ppm) and olefinic (5.3 ppm) peaks decreased, with respect to control. These results are in perfect agreement with a previous study from our group (Xavier et al, 2019b) where we found a similar trend in these peaks with disease progression following Western diet. The olefinic (5.3 ppm), allylic (2.0 ppm) and bulk methylene (1.3 ppm) peaks are somehow related to this change in PUFA and MUFA, because they correspond to FA with only one double bond and also the FA with no double bonds. The diallylic peak, corresponds only to FA with two or more double bonds. The decrease in PUFA observed by MRS was in agreement with results obtained by GC-MS. Decreased PUFA is of interest since the arachidonic (C20:4), eicosapentaenoic acid (C20:5) and docosahexaenoic acids (C22:6) are known precursors for a variety of anti- and pro- inflammatory mediators (Bazan, 2005).

Interestingly, from week 4 to 10 of CDAA diet intervention, the percentage of all peaks (found by MRS) did not change and neither the PUFA, MUFA, and SFA according to GC-MS analysis. This result shows that the data obtained by MRS and GC-MS are in perfect agreement. In contrast, a previous work of our group (Xavier et al, 2019b) using Western diet, showed a constant decrease in PUFA and increased in MUFA, but at that stage of the NAFLD disease, the mice had steatosis and early stages of NASH as you can see in Figure

3.6 and compare with Figure 3.3C, from this work. This result is very remarkable, since liver fatty acids composition has shown a very good correlation with NAFLD progression until NASH (Xavier et al, 2019b); however, during the NASH progression, our results suggest that the FA composition reach a plateau and does not show changes during the progression in this stage of the liver disease. The main reason why FA composition did not change with the progression of the disease in NASH stages is still unclear, but the hypothesis is that the PUFA decreases until they reach a certain limit and then, they cannot decrease anymore, nevertheless the liver continues to produce inflammation and fibrosis.

When NASH is generated, a variety of independent processes promote tissue inflammation and break the delicate balance of anti- and pro- inflammatory processes (Hirsova & Gores, 2015). For example, FA saturate the system and develop adipotoxicity in hepatocytes and resident macrophages, promoting injury and death of liver tissue by various mechanisms (Tilg & Moschen, 2010). For this reason, it is not necessary to increase FA in NASH to induce cytotoxicity, as we see in our animal model. On the other hand, PUFA are involved in anti-inflammatory processes; in NASH they decrease and are no longer able to counteract systemic and hepatic inflammation (Buechler & Aslanidis, 2020). In this scenario, the anti-inflammatory and pro-inflammatory balance in the liver with NASH is lost, and the disease progresses without necessarily presenting substantial changes in the different hepatic lipids once the inflammation in this organ has been established.

Another theory is based on the type of diet and regarding Figures 3.3C and 3.6, comparing the results obtained with the CDAA diet and Western diet. CDAA dietetic treatment has a pronounced inflammatory component in comparison to the Western Diet model. Thus, it is reasonable to not obtain the same behaviour shown in our previous work (Xavier et al, 2019b).

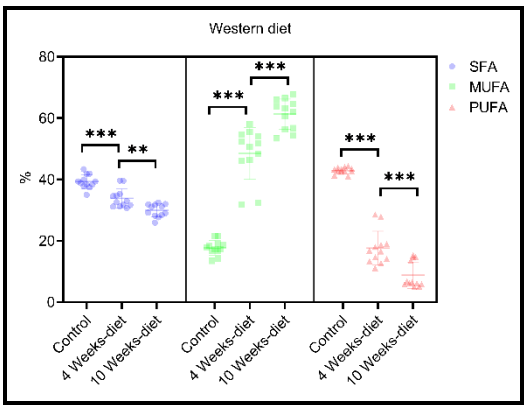

Figure 3.6. The relative contribution of each group of fatty acids: Saturated fatty acids (SFA: C14:0, C15:0, C16:0, C18:0), monounsaturated fatty acids (MUFA, C16:1, C18:1) and Polyunsaturated fatty acids (PUFA, C18:2, C18:3, C20:3, C20:4, C20:5 C22:6) for mice fed Western diet. Data from Western diet came from a previous work of our group.*$p < 0.05$, **$p < 0.01$, ***$p < 0.001$ (significant differences between groups). The date was taken from Xavier et al, (2019b)

The in-vivo spectra showed a linewidth bigger than ex-vivo, and this enlargement is explained because we made the in-vivo spectrum in the liver, which is an organ, so it is a solid material and we made the ex-vivo spectrum in a liquid solution with FAME and $CDCl_3$, and some effects could be compared between MRS in solids and liquids, like J-coupling, chemical shifts and magnetic susceptibility that results in an enlargement of the peak in solid materials (Claridge, 2016).

Besides that, the percentual of the metabolites had significant differences when comparing in-vivo with ex-vivo results, mainly with diallylic and allylic peaks, both are bigger in-vivo; however, the difference was not higher than 2%. This effect could be explained by the noise interference in the results as they are the smaller peaks. Also, in the case of in-vivo results, the allylic peak overlaps with α-methylene and could lead to a not optimal fitting, then a not exactly correct result.

Some works already studied in-vivo in comparison with ex-vivo in brain metabolites (for strokes and tumours) (Wilson et al, 2009), (Jiménez-Xarrié et al, 2015). None of them had a perfect agreement between the metabolites in-vivo and ex-vivo, but the ex-vivo results helped to explain the results obtained in-vivo. In our study, as mentioned before, we also obtained some differences in the value of peaks (less than 2%). However, six of seven peaks presented the same trend with the progression of the disease.

There are some limitations in our work that could be explored in the future. First, we performed all the experiments with a mice model, that is more stable. Therefore, the results might have some differences when compared to humans. However, the methodology used in this study can be transferred to human liver spectra. Second, we have used a surface coil in the in-vivo results, and we were not able to have access to all the liver. Therefore, we made the spectrum in only two voxels of the liver, and this limitation could be easily improved by changing the coil to a "whole body" coil and by doing more voxels in the liver to have a more representative result. This improvement could also make the results in-vivo more similar to ex-vivo

This study aimed to help the FA characterization of different NAFLD models, which seems to have clinical potential to monitor the progression of this disease. This work concluded that the FA do change from healthy (control) mice group to early stages of NASH, however they remain the same during the progression of NASH until some stages of fibrosis. The same conclusion was observed ex-vivo and in-vivo. The ex-vivo analysis was essential to validate the results with the GC-MS and the histology and helped to understand the trend of the in-vivo analysis.

4. TRANSLATIONAL STUDY WITH VOLUNTEERS AT 7 TESLA

This chapter is based on the article published in the journal NMR in Biomedicine, and was performed in collaboration with the Imaging Division, University Medical Center Utrecht, the Netherlands.

Xavier, A., Arteaga de Castro, C.S., Andia, M.E., Luijten, P. R., Klomp, D. W., Fillmer, A., and Prompers, J.J. (2020) Metabolite cycled liver 1H-MRS on a 7 T parallel transmit system. *NMR Biomed*, 33, E4343.

4.1 Introduction

Hepatic steatosis is a hallmark of non-alcoholic fatty liver disease (NAFLD), the most common liver disorder in the Western world, which can evolve into non-alcoholic steatohepatitis (NASH), liver cirrhosis, and hepatocellular carcinoma (Angulo, 2002), (Cohen et al, 2011). In addition to the highly elevated amounts of lipid in the liver, NAFLD is also associated with marked changes in liver lipid composition.

Localized ^{1}H magnetic resonance spectroscopy (MRS) has proven to be a reliable tool for the in-vivo quantification of lipid content in the liver, showing strong correlations with liver biopsy results (Hamilton et al, 2011), (Johnson et al, 2008), (Longo et al, 1995), (Reeder et al, 2011), (Szczepaniak et al, 2005). In addition, ^{1}H-MRS has been applied as a non-invasive method for the analysis of liver lipid composition based on the olefinic, diallylic and allylic lipid proton signals (Hamilton et al, 2011), (Jonhson et al, 2008), (Lundbom et al, 2011). However, at common clinical magnetic field strengths (1.5 – 3.0 T), the spectral resolution of liver ^{1}H MR spectra is limited, hampering accurate determination of lipid composition.

Ultra-high field (UHF; main magnetic field (B_0) ≥ 7.0 T) MRS provides increased spectral resolution, which should improve the reliability of the assessment of liver lipid composition. However, UHF-MRS in the liver is challenging because of large B_0 and transmit field (B_1^+) inhomogeneities. UHF-MRI systems are not equipped with a ^{1}H body transmit coil and hence local transmit coils have to be used. Gajdošík et al. have recently shown the application of ultrashort-TE stimulated echo acquisition mode (STEAM) MRS

for the quantification of liver lipid content and composition at 7 T using a surface coil for transmit and receive, which is associated with large B_1 inhomogeneities and limited penetration depth (Gajdosik et al, 2015). Recent advances in RF transmit coil array design have shown the beneficial use of fractionated dipole antennas for body imaging at UHF, providing increased transmit efficiency and homogeneity within the specific absorption rate (SAR) limits (Raaijmakers et al, 2016). Moreover, it was shown that combining dipole antennas with loop coils in receive arrays enhances the signal-to-noise ratio (SNR) compared to receiving with dipoles or loops only (Steensma et al, 2018). A setup consisting of fractionated dipole antennas combined with additional receive-only loops is therefore expected to be beneficial for liver MRS at 7 T, allowing measurements at various locations in the liver (e.g. anterior, lateral or posterior locations), including also less superficial parts.

An additional challenge for liver MRS is that respiratory and other physiologic and subject motion induces phase and frequency shifts, which leads to incoherent averaging and hence to suboptimal results. Metabolite cycling (MC) (Dreher & Leibfritz, 2005), (de Graaf et al, 2006), (MacMillan et al, 2011) has been proven beneficial, especially for small voxel volumes which are influenced by motion (Fillmer et al, 2017), (Giapitzakis et al, 2018), (Hock et al, 2013). MC makes use of an inversion pulse (Hwang & Zijl, 1999) to alternately invert the signal of the metabolites upfield or downfield of water, while leaving the water magnetization untouched. The advantage of the latter is that the unsuppressed water signal can be used for phase and frequency correction of the individual acquisitions, which is more accurate as compared to using the low-SNR metabolite signals in water-suppressed spectra. Subtraction of the upfield and downfield inverted spectra effectively cancels the water signal and, importantly, the gradient induced modulation sidebands, leaving a clean metabolite spectrum from which also low-concentration metabolites can be reliable quantified. The sum of the upfield and downfield inverted spectra, on the other hand, provides a water spectrum, which can be used as internal reference for quantification. These benefits of MC in combination with the application of parallel transmission technology and advanced RF coils enable the acquisition of high-quality UHF ^{1}H-MRS in the liver with a greater flexibility for positioning the volume of interest.

Here we show the application of MC for liver ^{1}H-MRS on a 7 T parallel transmit system, using 8 transmit-receive fractionated dipole antennas with 16 additional, integrated receive loops. Because of the short T_2 relaxation times in the liver at 7 T (Gajdosik et al, 2015), (Gajdosik et al, 2014), localization was performed with a short-TE STEAM sequence. The performance of MC-STEAM was compared with STEAM measurements with conventional water suppression using variable pulse powers and optimized relaxation delays (VAPOR) (Tkac et al, 1999) in healthy, lean volunteers. In addition, the effect of synchronized breathing was investigated in comparison with free breathing acquisitions and intra-session repeatability and inter-session reproducibility of liver lipid content as determined by the different acquisition methods were determined.

4.2 Subjects and methods

Data were acquired in a phantom containing a lipid emulsion (0.1 vol% Intralipid^{TM} soybean oil emulsion in water with 90 mM NaCl and 0.12 mM $MnCl_2$) and in the liver of six healthy, lean volunteers (age: 27-47 years; body mass index: 21.6-23.9 kg/m^2; 3 male, 3 female; Table 1). The study was approved by the local medical ethics committee and all subjects signed informed consent prior to inclusion. Each subject was scanned twice on two separate days, approximately one week apart. Conditions, such as nutrition and physical activity, were not standardized.

Table 4.1 Subjects' characteristics

Subject	Sex	Age (years)	BMI (kg/m^2)
1	male	37	23.0
2	male	27	23.0
3	male	44	21.6
4	female	36	22.3
5	female	28	23.9
6	female	47	23.3

BMI: body mass index.

4.2.1 Data acquisition

All measurements were performed on a 7 T Philips Achieva multi-transmit system (Philips Healthcare, Best, the Netherlands) with a maximal gradient amplitude of 40 mT/m at a

slew rate of 200 T/m/s, using 8 parallel transmit channels driven by 8 x 2 kW peak power amplifiers. Each transmit channel was connected to a transmit-receive fractionated dipole antenna (Raaijmakers et al 2016) with two additional integrated receive-only loops (MR Coils BV, Zaltbommel, the Netherlands), resulting in an 8-channel transmit/24-channel receive setup (Steensma et al, 2018). The 16 receive-only loops were interfaced to a 16-channel receiver box.

First, T_1 weighted gradient echo localizer images were acquired. Then, low-flip-angle gradient echo images (2D multi-slice acquisition, TE = 1.68 ms, TR = 30 ms, FOV = 350 × 457 × 30 mm^3, in-plane resolution = (3.9 × 3.8) mm^2, slice thickness = 10 mm, flip angle = 3.5°) were acquired in three slices in the liver for every transmit channel, which were used for RF phase shimming (Metzger et al, 2008). Optimum phase settings to obtain maximum signal intensity in a region of interest (ROI) in the right lobe of the liver (averaged over three slices) were calculated with a numerical minimization in Matlab (Mathworks, Natick, MA, USA). Amplitudes of the channels were all set equally. For both the phantom and the in-vivo measurements, RF phase shimming resulted in a B_1^+ of 16-19 μT in the ROI, which was quantified from a B_1 map measured using the actual flip angle imaging (AFI) method (Yarnykh, 2007) (3D gradient echo, TE = 2.3 ms, TR = 50 and 250 ms, FOV = 280 × 420 × 30 mm^3, resolution = (3.9 × 3.8 × 10) mm^3, flip angle = 55°). A 3D B_0 map (3D gradient echo, TE = 1.49 ms, ΔTE = 1.0 ms, TR = 10 ms, FOV = 280 × 402 × 78 mm^3, resolution = (4.4 × 6.0 × 6.0) mm^3, flip angle = 5°) was acquired during a breath hold in the exhaled state (acquisition time = 16.3 s) for B_0 shimming. Linear and second order shim settings were optimized over the ROI in the right lobe of the liver, while a region of less interest covering the whole liver was also considered during the calculation, albeit with a lower weight (Fillmer et al, 2015), using the MRCode software (MR Code BV, Zaltbommel, the Netherlands). A DIXON (Dixon, 1984) scan (2D multi-slice gradient echo, TE = 2.6 ms, ΔTE = 0.5 ms, TR = 10 ms, FOV = 282 × 360 × 80 mm^3, in-plane resolution = (1.3 × 1.3) mm^2, slice thickness = 4 mm, 20 slices, flip angle = 15°) was performed after RF phase and B_0 shimming, which was used for planning of the MRS voxel.

STEAM spectra were acquired in a 15 × 15 × 20 mm^3 voxel positioned in the right lobe of the liver, in the same region where B_1 and B_0 fields were optimized. Major vessels and

biliary structures (more concentrated in the deeper lying regions of the liver) and edges of the liver were avoided, while taking care that voxels for both the water and lipid methylene frequencies were surrounded by homogeneous, liver tissue. Spectra were acquired with water suppression using VAPOR (100 Hz bandwidth for the phantom and 200 Hz bandwidth for the in-vivo liver measurements), including a water reference scan, and without water suppression using MC. For the latter, the STEAM sequence was modified to include an asymmetric adiabatic MC inversion pulse (Hwang & Zijl, 1999) in the mixing period (Dreher & Leibfritz, 2005), (Giapitzakis, 2018) (MC pulse duration = 22.4 ms). The offsets for the MC pulses were +175 Hz and -175 Hz from the water frequency for odd and even scans, respectively. In the phantom, also a MC-STEAM spectrum was recorded with MC pulse offsets of +50 Hz and -50 Hz, for a more fair comparison with the VAPOR-STEAM spectrum with a 100 Hz bandwidth for the VAPOR water suppression. Other scan parameters for the MRS measurements were as follows: spectral bandwidth = 4000 Hz, data points = 1024, TE = 10 ms, TM = 38 ms, TR = 2500 ms, N_{avg} = 64/128 (phantom/liver). For the in-vivo measurements, in each session both VAPOR-STEAM and MC-STEAM spectra were acquired once with free breathing and twice with synchronized breathing, resulting in 6 MRS measurements per session. For the measurements with synchronized breathing, the volunteers were instructed to synchronize their breathing with the sound of the applied sequence, such that acquisitions were performed in the exhaled state. The repeated measurements with synchronized breathing within each session (both for VAPOR-STEAM and MC-STEAM) were used to determine the intra-session repeatability of the quantification of liver lipid content. For each subject, the whole scan protocol was repeated on two different days, approximately one week apart, to determine the inter-session reproducibility. Care was taken to keep the positioning of the MRS voxel as constant as possible between sessions, which was guided by anatomical landmarks.

4.2.2 Data processing and quantification

The signals of the individual acquisitions (one per TR) of the 24 channels (8 transmit-receive fractionated dipole antennas and 16 receive loops) were individually phased and Eddy current corrected before channel combination, frequency alignment and averaging,

using an in-house written Matlab script (Mathworks, Natick, MA, USA). Eddy current correction of the VAPOR-STEAM data was performed using the water reference scan. Channel combination was performed using the generalized least squares (GLS) algorithm (An et al, 2013), using all averages for the MC-STEAM scans or only the water reference scan for the VAPOR-STEAM measurements. After channel combination, frequency alignment was performed based on frequency domain correlation (Wiegers et al, 2017). For the MC-STEAM spectra, correlations were calculated for the spectral region containing the water peak, while for the VAPOR-STEAM spectra the spectral region to calculate the correlations included the lipid methyl signal (0.90 ppm) up to the signal from choline containing compounds (3.22 ppm). For the MC-STEAM spectra, signals were separately averaged for the odd and even acquisitions, which were then summed and subtracted, to yield the water and metabolite signals, respectively.

Spectra were fitted with the Advanced Method for Accurate, Robust and Efficient Spectral fitting (AMARES) in the jMRUI software package (Stefan et al, 2009), (Vanhamme et al, 1997) without any further post-processing, such as apodization or removal of the residual water signal in the metabolite spectra. In the water spectra, the water signal was fitted by a single Lorentzian line. In the metabolite spectra, the lipid resonances at 5.30 (olefinic methine, -C***H***=C***H***-), 2.77 (diallylic methylene, -CH=CH-C***H***$_2$-CH=CH-), 2.24 (α-carboxylic methylene, -C$_\alpha$***H$_2$***-COO-), 2.02 (allylic methylene, -C***H***$_2$-CH=CH-C***H***$_2$-), 1.62 (β-carboxylic methylene, -C$_\beta$***H$_2$***-CH$_2$-COO-), 1.30 (methylene, (-C***H***$_2$-)$_n$) and 0.90 (methyl, -C***H***$_3$) ppm and the signal from choline containing compounds (total choline, tCho) at 3.22 ppm were fitted by Lorentzian lines with equal line widths. To make the fitting more robust, amplitudes of the α-carboxylic methylene, β-carboxylic methylene and methyl peaks at 2.24, 1.62 and 0.90 ppm were constrained to have ratios of 1 : 1 : 1.33, as theoretically predicted from the number of protons and the T_1 and T_2 relaxation time constants (Gajdosik et al, 2014). For the MC-STEAM spectra, fitting of the olefinic methine peak at 5.3 ppm was omitted.

Liver lipid content was calculated as L/(L + W) * 100%, where W represents the amplitude of the water signal (in the time domain; corresponds to the integral in the frequency domain) and L the total amplitude of the following lipid signals: diallylic methylene, α-

carboxylic methylene, allylic methylene, β-carboxylic methylene, methylene, and methyl (2.77, 2.24, 2.02, 1.62, 1.30 and 0.90 ppm). Signals were corrected for T_1 and T_2 relaxation using the relaxation time constants as determined by Gajdošík et al. (2014). The unsaturation index (UI) was calculated according to Johnson et al. (2008) as the ratio of the sum of the amplitudes of the diallylic and allylic methylene signals (2.77 and 2.02 ppm) to the sum of the amplitudes of the diallylic methylene, allylic methylene, methylene and methyl signals (2.77, 2.02, 1.30 and 0.90 ppm), corrected for T_1 and T_2 relaxation.

4.2.3 Statistical analysis

Data are presented as means ± standard deviation (SD). The data have normal distribution as confirmed by Shapiro-Wilk test. Statistical significance of differences between reconstruction without and with frequency correction, measurements with free and synchronized breathing (using the first synchronized scans), and measurements with VAPOR-STEAM and MC-STEAM were assessed by applying a three-way Analysis of Variance (ANOVA), followed by Bonferroni corrected post-hoc tests using the IBM SPSS 25.0 statistical package (SPSS Inc., Chicago, IL, USA). Differences between repeated measurements within one session and repeated measurements between two sessions were assessed using paired samples *t*-tests. Statistical significance was set at $p < 0.05$.

Comparisons of liver lipid content measured with free and synchronized breathing and with VAPOR-STEAM and MC-STEAM were made using Bland-Altman analyses. Intra-session and inter-session variability of liver lipid content were also assessed using Bland-Altman analyses. Coefficients of repeatability/reproducibility (CR) were calculated from the SD of the signed differences between two scans for each subject according to CR = 1.96 x SD. Coefficients of variation (CVs) were calculated as the SD of the differences divided by the mean. Correlation between unsaturation index (UI) and liver lipid content was assessed using Pearson's correlation.

4.3 Results

4.3.1 Phantom measurements

Figure 4.1A-C compares VAPOR-STEAM and MC-STEAM spectra recorded on the phantom with a lipid emulsion. Using MC-STEAM, the subtraction of downfield and upfield inverted spectra led to a spectrum free of sidebands, with good water cancellation. However, the olefinic lipid signal, which is close to the water peak (5.3 ppm), could not clearly be observed in the MC-STEAM spectrum with MC pulse offsets of +175 Hz and -175 Hz (Figure 4.1B), which were also used for the in-vivo measurements), whereas the (inverted) peak is clearly resolved in the MC-STEAM spectrum with MC pulse offsets of +50 Hz and -50 Hz (Figure 4.1C). The signal intensities of the other lipid resonances were comparable for VAPOR-STEAM and MC-STEAM. By varying the power for the asymmetric adiabatic MC inversion pulse, it was shown that a B_1^+ above 15 μT in the region of interest is required for complete inversion of the lipid methylene signal at 1.30 ppm and thus to obtain the full signal amplitude in the difference spectra (Figure 4.1D). This condition was met for all in-vivo measurements.

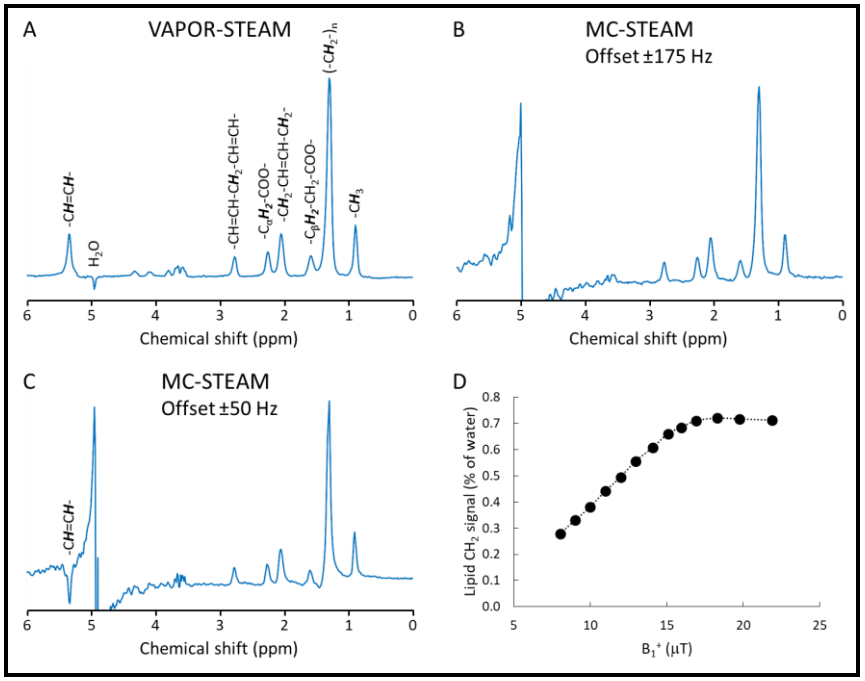

Figure 4.1. Spectra acquired in a phantom containing a lipid emulsion using (A) a conventional STEAM sequence and VAPOR water suppression, and (B and C) MC-STEAM without water suppression. In (B) the offsets for the MC pulses were +175 Hz and -175 Hz from the water frequency for odd and even scans, respectively (in-vivo settings), while in (C) the offsets for the MC pulses were +50 Hz and -50 Hz from the water frequency. All major lipid peaks in the upfield spectrum can be clearly identified within all spectra and are indicated in panel (A). The olefinic lipid signal at 5.3 ppm, however, can only be distinguished clearly in the VAPOR-STEAM spectrum (A) and in the MC-STEAM spectrum with the smaller offsets (C; olefinic lipid signal has a 180 degrees phase difference with the upfield signals). (D) Lipid methylene signal amplitude (expressed as a percentage of the water signal) as a function of the B_1^+ used for the MC pulses. A B_1^+ above 15 μT in the region of interest is required for complete inversion of the methylene signal and thus to obtain the full signal amplitude in the difference spectra.

4.3.2 In-vivo measurements

Figure 4.2 shows an example of the voxel positioning for the in-vivo liver measurements, as well as the results for the MC-STEAM acquisition. In Figure 4.2B the downfield and upfield inverted spectra (after individual phase correction, coil combination, frequency alignment and averaging) are separately displayed, showing an excellent efficiency of the MC inversion pulse. The sum of the downfield and upfield inverted spectra (Figure 4.2C) shows a clean water spectrum, whereas the difference of the downfield and upfield inverted spectra (Figure 4.2D) represents the metabolite spectrum.

Figure 4.3 compares VAPOR-STEAM and MC-STEAM spectra acquired in-vivo in the liver from the voxel indicated in Figure 4.2A, both during free breathing and synchronized breathing and reconstructed without and with frequency correction. The positive effect of both synchronized breathing and frequency correction on lineshape and linewidth can be clearly observed in the data sets of this volunteer. Figure 4.4 shows the same type of data for a different subject, with a 2.3-fold lower liver lipid content as compared to the subject in Figure 4.3 (1.0% vs. 2.3%). In this case, it is evident that frequency correction no longer leads to an improvement of the VAPOR-STEAM spectra, and in fact leads to worse lineshapes, while for the MC-STEAM spectra frequency alignment still leads to a significant enhancement of the spectral quality. For the subjects with a liver lipid content below 2%, frequency correction of the VAPOR-STEAM spectra did not give optimal results in 54% of the cases, while the effect of frequency alignment of the water signal in the MC-STEAM spectra on the metabolite difference spectra was satisfactorily in all cases.

Figure 4.5 shows the quantification of the SNR of the lipid methylene peak (1.30 ppm) and the linewidth of the lipid peaks for all 6 subjects for both scan sessions. Frequency alignment did significantly improve the SNR for the data with free breathing, but not for synchronized breathing (Figure 4.5A). SNR was not significantly different between the spectra measured with free and synchronized breathing or between the spectra acquired with VAPOR-STEAM and MC-STEAM. Linewidths became significantly smaller when frequency alignment was applied before averaging the individual acquisitions (Figure 4.5B), both for the VAPOR-STEAM and the MC-STEAM scans and both for free breathing and for synchronized breathing, although the effect was smaller for synchronized breathing. Linewidths also significantly improved with synchronized breathing as compared with free breathing, both for VAPOR-STEAM and MC-STEAM and both without and with frequency correction. However, with frequency alignment, the effect of synchronized breathing on the linewidths was less pronounced.

For the remainder of the results, we only consider the data that were reconstructed with frequency correction. Figure 4.6 shows Bland-Altman analyses for comparisons of liver lipid content between scans with free breathing and synchronized breathing acquired with VAPOR-STEAM (A) and MC-STEAM (B) and for comparisons between scans of VAPOR-STEAM and MC-STEAM obtained with free breathing (C) and synchronized

breathing (D). The difference between free breathing and synchronized breathing acquisitions was smaller for MC-STEAM than for VAPOR-STEAM (CV = 8.3% vs. 14.1%), but for both acquisition methods there were no significant differences in liver lipid content between free and synchronized breathing. The CV between VAPOR-STEAM and MC-STEAM was 14.4% for free breathing acquisitions and 20.0% for synchronized breathing acquisitions. Differences in lipid content between VAPOR-STEAM and MC-STEAM were not significant both for free and synchronized breathing.

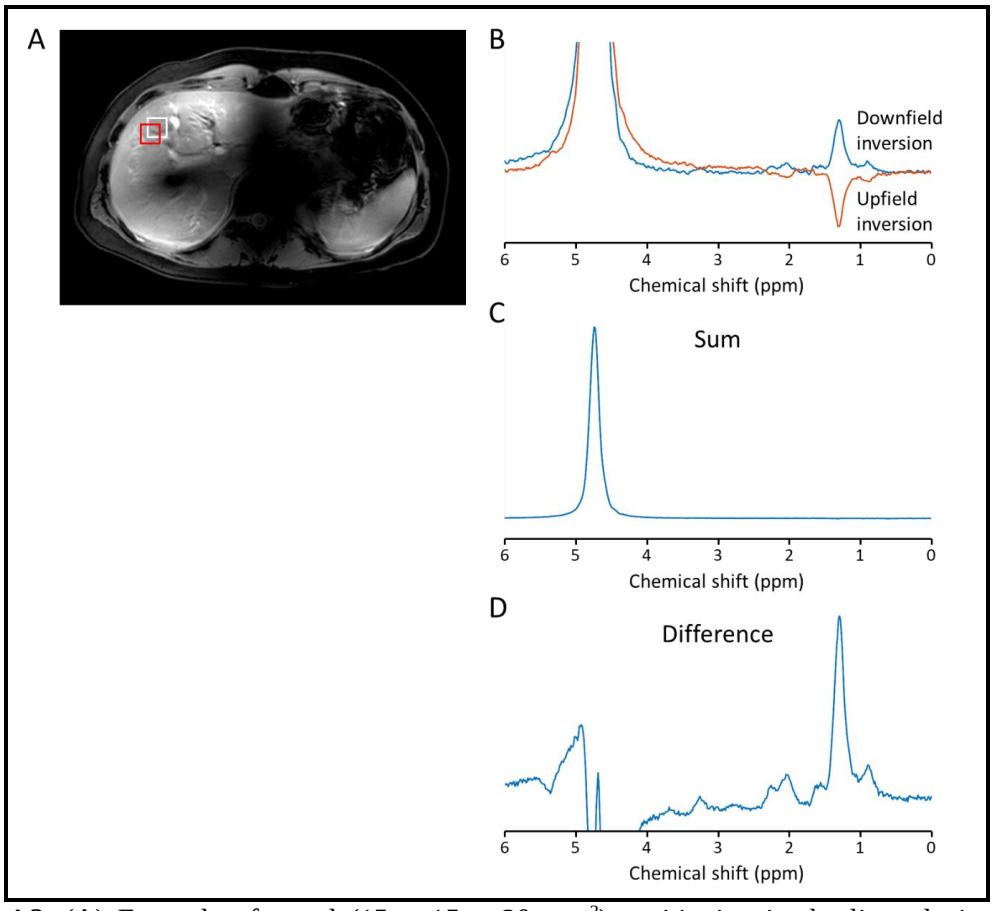

Figure 4.2. (A) Example of voxel (15 × 15 × 20 mm^3) positioning in the liver depicted on a transversal DIXON scan. The red voxel indicates the voxel positioning for the water frequency, while the white voxel indicates the shifted voxel for the lipid methylene frequency. (B-D) In-vivo liver spectra from the voxel indicated in (A) using MC-STEAM: (B) displays the downfield (blue) and upfield (red) inverted spectra (after individual phase correction, coil combination, frequency alignment and averaging); (C) shows the sum of the downfield and upfield inverted spectra (water spectrum); and (D) the difference (metabolite) spectrum.

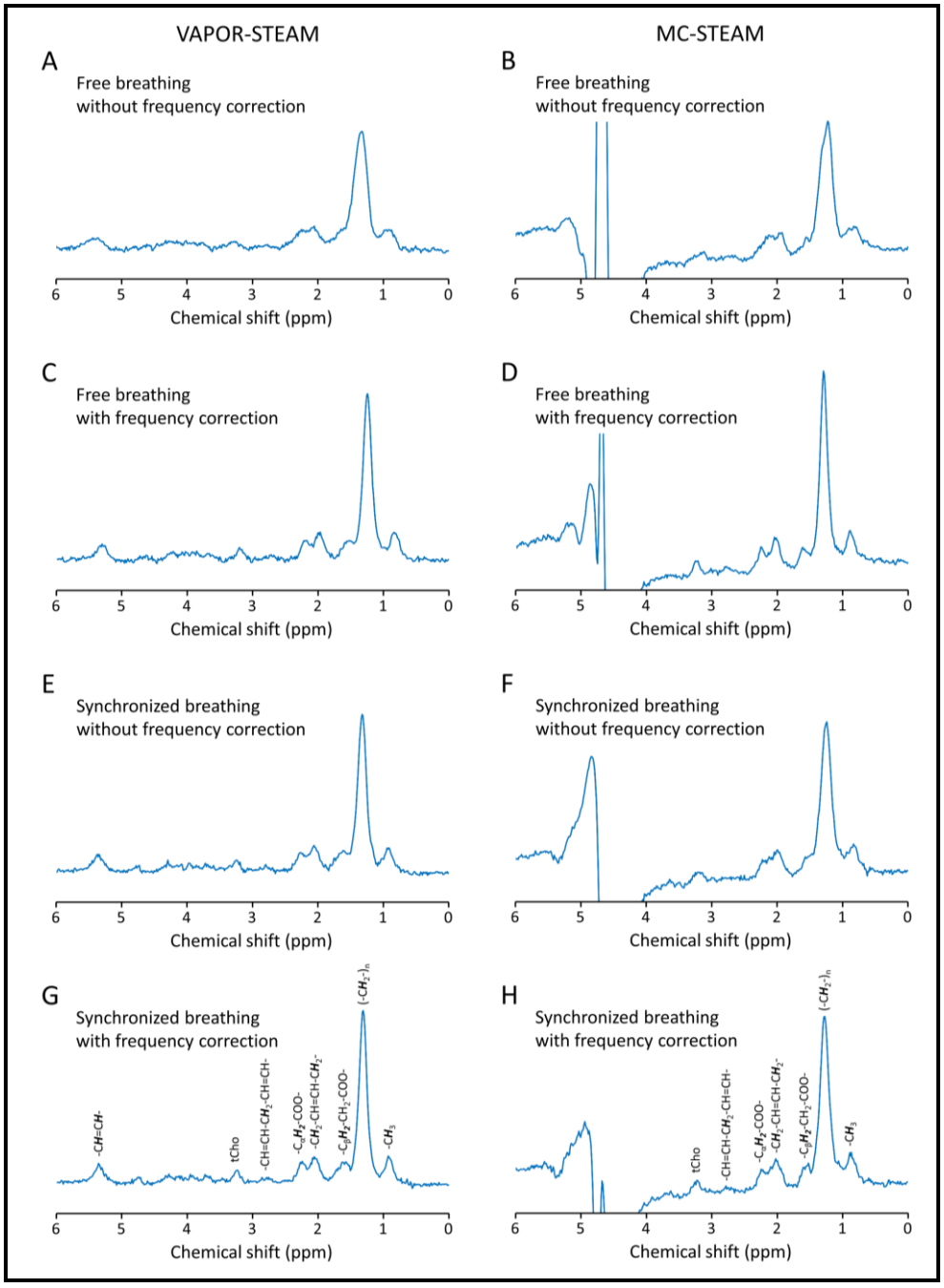

Figure 4.3. Comparison of in-vivo liver spectra from the voxel indicated in Figure 4.2A (all in the same subject) recorded using VAPOR-STEAM (left column) and MC-STEAM (right column) with free breathing reconstructed without frequency correction (A and B) and with frequency correction (C and D) and with synchronized breathing reconstructed without frequency correction (E and F) and with frequency correction (G and H). Peak assignments are indicated in panels (G) and (H). The peak at 3.22 ppm (not present in the phantom spectra) originates from choline containing compounds (total choline, tCho). Liver lipid content for this subject averaged over the different spectra was 2.3%.

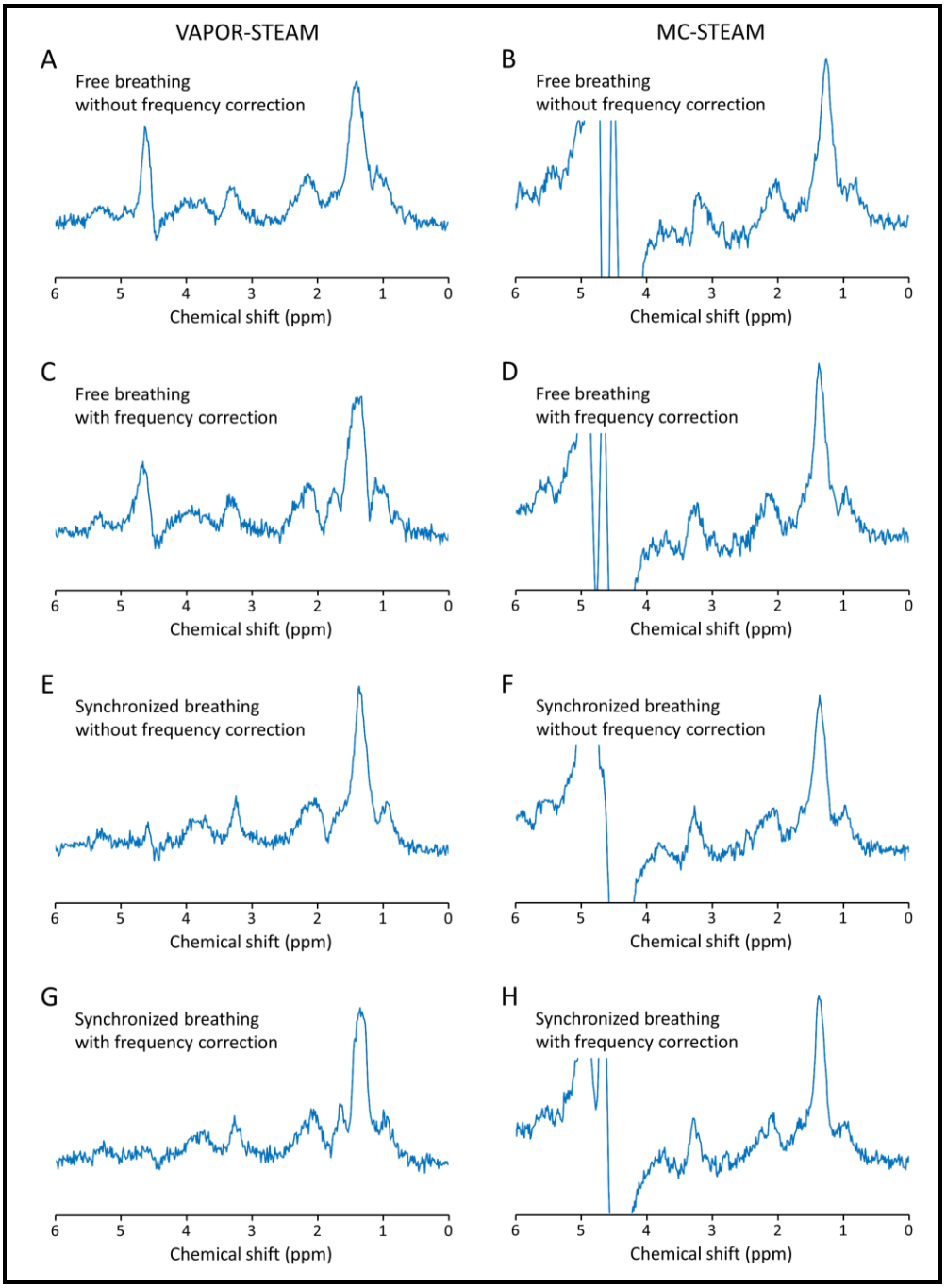

Figure 4.4. Comparison of in-vivo liver spectra from another subject, with a lower liver lipid content as compared to the subject in Figure 4.3, recorded using VAPOR-STEAM (left column) and MC-STEAM (right column) with free breathing reconstructed without frequency correction (A and B) and with frequency correction (C and D) and with synchronized breathing reconstructed without frequency correction (E and F) and with frequency correction (G and H). Liver lipid content for this subject averaged over the different spectra was 1.0%.

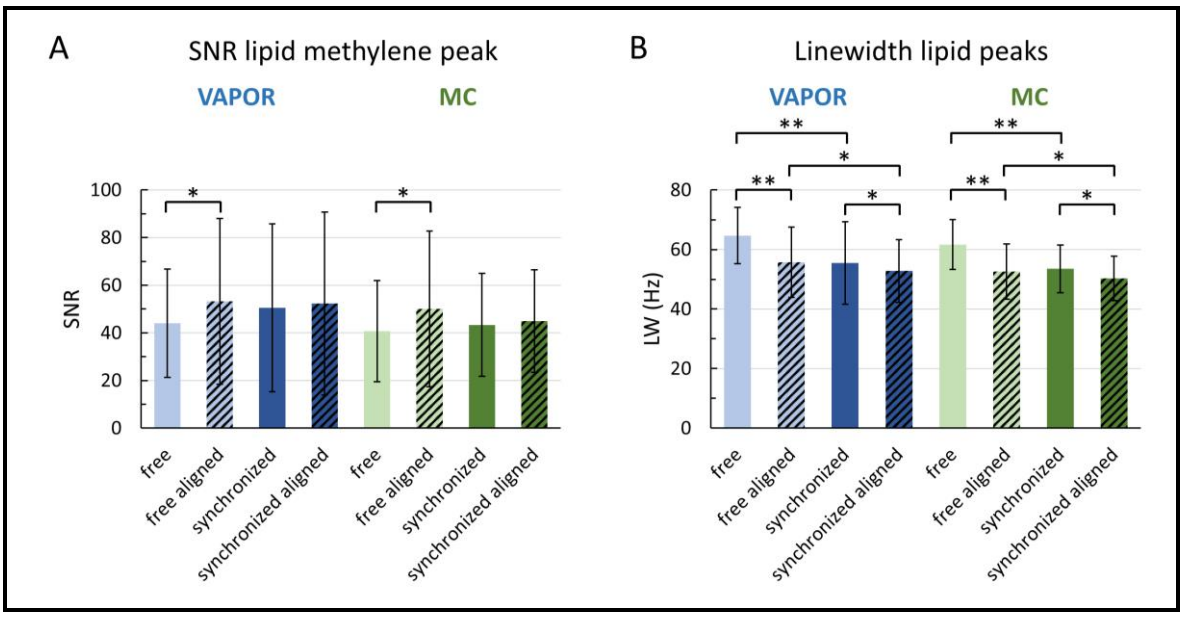

Figure 4.5. (A) Average signal-to-noise ratio (SNR) for the lipid methylene peak (1.30 ppm) and (B) linewidth (LW) of the fitted lipid peaks for the 6 subjects for both scan sessions from acquisitions with VAPOR-STEAM with free breathing (light blue) and synchronized breathing (dark blue), and MC-STEAM with free breathing (light green) and synchronized breathing (dark green). Results are shown for data reconstructed without (uniform colored bars) and with (colored bars with black hatches) frequency correction. For both SNR and LW, there was no significant difference between VAPOR and MC, but there was a significant interaction between the effects of reconstruction without and with frequency correction and measurements with free and synchronized breathing ($p=0.04$ and $p=0.03$ for SNR and LW, respectively). The significance signs in the figure represent the results of the Bonferroni corrected post-hoc tests for the pooled VAPOR and MC data. *$p<0.05$, *$p<0.01$.

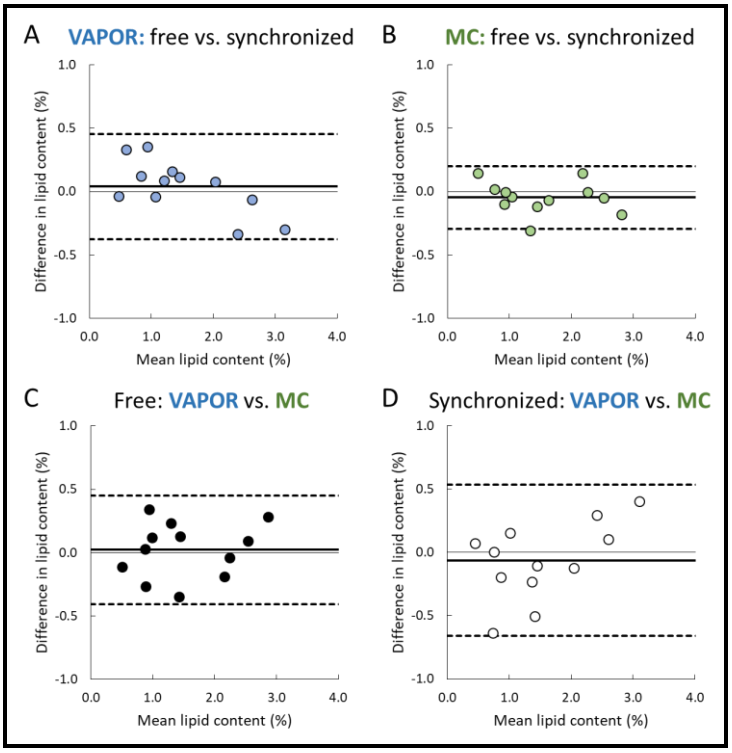

Figure 4.6. Bland-Altman plots for comparisons of liver lipid content between scans with free breathing and synchronized breathing acquired with VAPOR-STEAM (A) and MC-STEAM (B) and for comparisons between scans with VAPOR-STEAM and MC-STEAM obtained with free breathing (C) and synchronized breathing (D). Spectra were reconstructed with frequency correction. Solid black line shows the bias from zero (thin black line) and dashed black lines mark ±1.96 SD. (A) absolute bias = 0.04%, CR = 0.42%, CV = 14.1%; (B) absolute bias = 0.05%, CR = 0.25%, CV = 8.3%; (C) absolute bias = 0.02%, CR = 0.45%, CV = 14.4%; (D) absolute bias = 0.06%, CR = 0.60%, CV = 20.0%.

4.3.3 Intra-session repeatability

For the acquisitions with synchronized breathing, the intra-session repeatability of the quantification of liver lipid content was determined during both sessions (Figure 4.7). Intra-session variability was smaller for MC-STEAM (CV = 9.6%) than for VAPOR-STEAM (CV = 12.2%). Furthermore, for MC-STEAM there was no bias from zero, while for VAPOR-STEAM there was a small bias (absolute bias = -0.06%). For both methods, there were no significant differences in liver lipid content between repeated measurements in the same subjects.

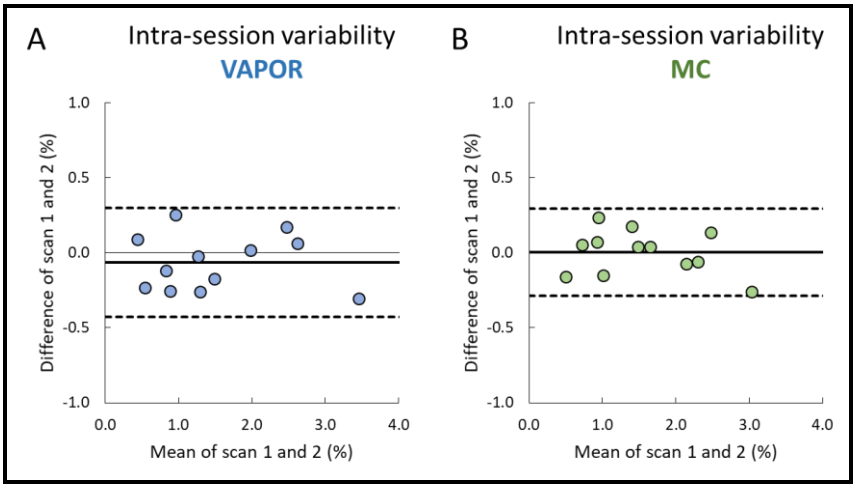

Figure 4.7. Bland-Altman plots of intra-session variability in liver lipid content measured with VAPOR-STEAM (A) and MC-STEAM (B) with synchronized breathing. Spectra were reconstructed with frequency correction. Solid black line shows the bias from zero (thin black line) and dashed black lines mark ±1.96 SD. (A) absolute bias = 0.06%, CR = 0.36%, CV = 12.2%; (B) absolute bias = 0.00%, CR = 0.29%, CV = 9.6%.

4.3.4 Inter-session reproducibility

In addition, the inter-session reproducibility of liver lipid content quantification was determined for both free breathing and synchronized breathing conditions (Figure 4.8). Inter-session variability was smaller for MC-STEAM (CV = 23.2% and 29.4% for free and synchronized breathing, respectively) than for VAPOR-STEAM (CV = 37.1% and 39.5% for free and synchronized breathing, respectively) and was comparable for the scans with free and synchronized breathing. For both methods, there were no significant differences in liver lipid content between repeated measurements in the same subjects.

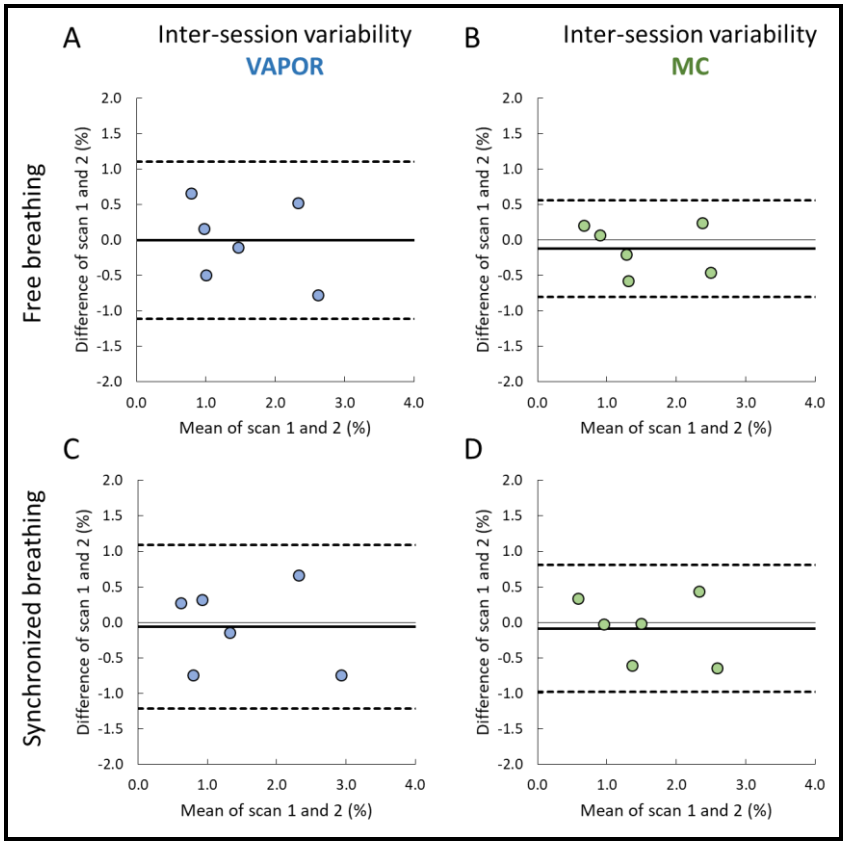

Figure 4.8. Bland-Altman plots of inter-session variability in liver lipid content measured with VAPOR-STEAM (A, C) and MC-STEAM (B, D) with free breathing (A, B) and synchronized breathing (C, D). Spectra were reconstructed with frequency correction. Solid black line shows the bias from zero (thin black line) and dashed black lines mark ±1.96 SD. (A) absolute bias = 0.01%, CR = 1.11%, CV = 37.1%; (B) absolute bias = 0.12%, CR = 0.68%, CV = 23.2%; (C) absolute bias = 0.06%, CR = 1.15%, CV = 39.5%; (D) absolute bias = 0.09%, CR = 0.90%, CV = 29.4%.

4.3.5 Lipid unsaturation

For the acquisitions with synchronized breathing, the intra-session repeatability of the quantification of the unsaturation index (UI) of hepatic lipids was determined during both sessions (Fig. 4.9A,B). Intra-session variability was smaller for MC-STEAM (CV = 17.2%) than for VAPOR-STEAM (CV = 51.7%). Figure 4.9 also shows the relation between UI and the liver lipid content, as measured with VAPOR-STEAM and MC-STEAM with synchronized breathing (Fig 4.9.C,D). For MC-STEAM, there was a negative linear correlation between UI and lipid content (R=-0.69, p=0.01), whereas for VAPOR-STEAM UI and lipid content were not significantly correlated (p=0.24).

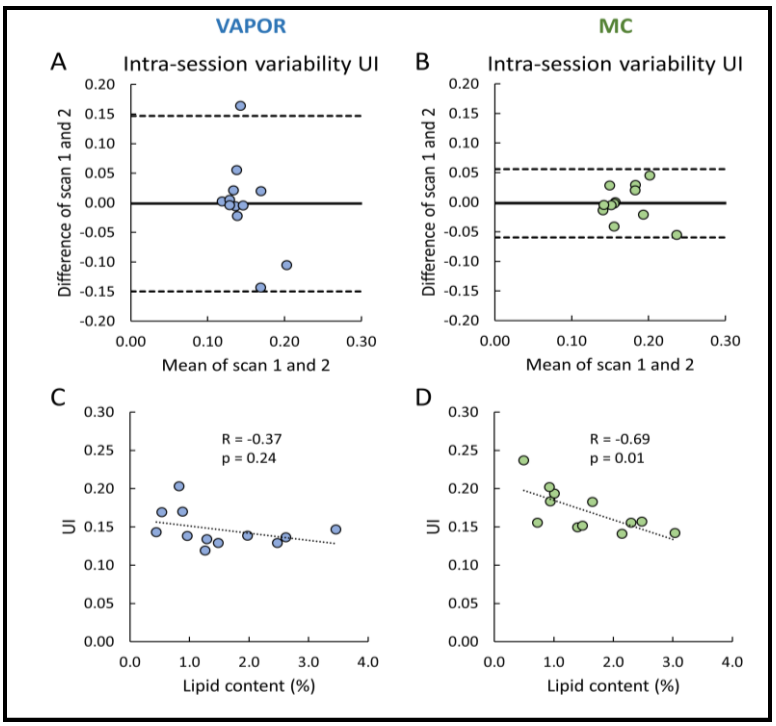

Figure 4.9. A,B: Bland-Altman plots of intra-session variability in unsaturation index (UI) of hepatic lipids measured with VAPOR-STEAM (A) and MC-STEAM (B) with synchronized breathing. Spectra were reconstructed with frequency correction. Solid black line shows the bias from zero (thin black line) and dashed black lines mark ±1.96 SD. (A) absolute bias = 0.00, CR = 0.15, CV = 51.7%; (B) absolute bias = 0.00, CR = 0.06, CV = 17.2%. C,D: UI versus liver lipid content for the 6 subjects for both scan sessions. Data were measured with VAPOR-STEAM (C) and MC-STEAM (D) with synchronized breathing and results of the two measurements acquired during one session were averaged. With MC-STEAM a significant negative correlation was observed, while the data acquired with VAPOR-STEAM did not indicate a clear relationship.

4.4 Discussion

In this study, the successful implementation of MC-STEAM for liver ^{1}H-MRS on a 7 T parallel transmit system, using 8 transmit-receive fractionated dipole antennas with 16 additional, integrated receive loops was demonstrated, and the performance was compared to that of STEAM measurements using VAPOR water suppression. After phase and frequency correction of the individual acquisitions (before averaging), spectra acquired with free breathing were of similar quality as compared with spectra from measurements during which the subjects synchronized their breathing with the acquisitions. Intra- session repeatability and inter-session reproducibility of liver lipid quantification were better for MC-STEAM than for VAPOR-STEAM. These effects may be explained by the more robust phase and frequency correction of the individual MC-STEAM acquisitions as

compared to the VAPOR-STEAM acquisitions, for which the low SNR lipid signals had to be used for these corrections.

Up to date, at 7 T, liver ^{1}H-MRS has only been applied using a relatively small surface coil for both transmit and receive (Gajdosik et al, 2015), (Gajdosik et al, 2014). Such a setup suffers from large B_1 inhomogeneities and penetration depth is very limited. By using 8 transmit-receive fractionated dipole antennas with 16 additional, integrated receive loops on a parallel transmit system and by applying RF phase shimming, we obtained high-quality images in which the whole liver anatomy was clearly visible (Figure 4.2A). This provided more freedom for and a better definition of the positioning of the MRS voxel. For the MC-STEAM spectra, adding the signals from the 16 receive loops increased the SNR by a factor of 1.9 on average as compared to using the signals from the 8 dipole antennas only, which is in good correspondence with previous MRI data with this setup (Steensma et al, 2018).

In the previously reported study, Gajdošík et al. presented an elegant approach to acquire ultrashort-TE STEAM ^{1}H MR spectra in the liver at 7 T without water suppression, with switching of the spoiler gradients for sideband reduction (Gajdosik et al, 2015). The water resonance was removed from the lipid spectra during post-processing, which involved fitting of the water resonance by multiple Lorentzian lines which were subsequently subtracted from the spectra. During an MC-measurement, the water signal is also retained, allowing for robust phase and frequency correction. Subtraction of downfield and upfield inverted spectra leads to a spectrum in which most of the water signal is canceled out and which is also free of gradient induced modulation sidebands. As such, MC presents an alternative method for non-water-suppressed liver ^{1}H-MRS as compared to the approach presented by Gajdošík et al. However, the in-vivo MC-STEAM difference spectra did not resolve the olefinic lipid signal at 5.3 ppm, while this signal could readily be detected in most in-vivo VAPOR-STEAM spectra. The culprit for this was the larger bandwidth of the frequency range untouched by the MC pulses of 350 Hz compared to the VAPOR water suppression bandwidth of 200 Hz for the in-vivo measurements.

We refrained from reducing the bandwidth of the non-inverted frequency range in the in-vivo MC experiments, since it is important not to affect the water signal by the MC pulses, if the water signal is to be used for quantification. In phantom measurements, reducing the

bandwidth of the non-inverted frequency range from 350 Hz to 100 Hz resolved the olefinic lipid signal (Fig. 1B,C), but also reduced the water signal amplitude by 13%. In the presence of frequency shifts due to motion, reducing the bandwidth of the non-inverted frequency range will likely lead to even greater reductions in water signal amplitude. Another reason not to shift the offsets for the MC pulses closer to the water frequency is that it would increase the required B_1^+ for full inversion of the lipid methylene peak (which was 15 μT for an offset of 175 Hz), which may not be achieved in all cases. Moreover, even though the olefinic lipid signal could be detected in most VAPOR-STEAM spectra, phantom measurements using the same water suppression bandwidth (200 Hz) as in the in-vivo experiments show that the olefinic peak amplitude was 23% lower and thus partially suppressed as compared with a VAPOR bandwidth of 100 Hz. Therefore, we decided not to use the olefinic lipid signal for quantification.

While the simultaneous acquisition of both water and metabolite signals is an advantage of MC, it also presents a limitation. When water and metabolite signals are acquired in separate acquisitions, the frequency offset is typically adjusted between the two scans to minimize the chemical shift displacement error (CSDE) between water and the metabolite of interest. With MC, this is not possible and the resulting CSDE between the voxel positioning for the water and lipid frequencies (Fig. 2A) could therefore potentially compromise the quantification of the lipid signals with respect to the water signal. However, during voxel planning we took the CSDE into account and we assumed that the liver tissue composition across the area covering the voxels at the water and lipid methylene frequencies was homogeneous enough to allow for meaningful quantification of the results.

For the MC-STEAM acquisitions, the robust phase and frequency correction of individual acquisitions using the water signal resulted in spectra with similar SNR and linewidths for measurements with free breathing and measurements with synchronized breathing. The variability between liver lipid content determined from MC-STEAM spectra measured with free and synchronized breathing (CV = 8.3%) was in fact comparable to the intra-session variability with synchronized breathing (CV = 9.6%). The voxel that we used for the MRS measurements was rather small (15 × 15 × 20 mm^3) and was surrounded by homogeneous, liver tissue. Therefore, even in the case of motion, the voxel was likely still

within liver tissue. It should be noted though that the possibility of not quite homogenously distributed lipids and lipid compositions within the liver will influence the measurement uncertainty introduced by subject motion during the measurement. Obviously, in smaller and/or less homogeneous organs, motion could lead to inaccurate results and synchronized breathing or some sort of gating would be required. Nonetheless, the finding that, in the liver, MC-STEAM with free breathing performs equally well as MC-STEAM with synchronized breathing indicates that MC-STEAM does not require synchronization with respiratory motion, and that the robust phase and frequency correction enabled by MC is able to compensate for additional measurement uncertainties introduced by subject motion. Especially in clinical settings, where patients may struggle with holding their breath or breathing in a very controlled way throughout the rather lengthy MRS measurements,this is very useful. In the studies of Gajdošík et al. (2014, 2015), volunteers were placed on the surface coil in a right lateral position to minimize abdominal motion and instructed to breathe flatly and regularly, which may not be feasible for patients either. The use of a respiratory belt or navigator for real-time or retrospective respiratory gating is also not without problems (e.g. loss of signal from respiratory belt or low quality navigator signal because of B_0 and B_1 inhomogeneities, especially at high field) and leads to increased scan times (Peereboom, 2019).

For the VAPOR-STEAM spectra, the performance of the frequency correction was not optimal in 54% of the data sets for subjects with liver lipid contents lower than 2%, even though this was not directly apparent from the SNR and linewidth figures. The variability between liver lipid content measured with free and synchronized breathing was higher for VAPOR-STEAM (CV = 14.1%) than for MC-STEAM (CV = 8.3%). Also, intra-session variability for liver lipid content quantification with VAPOR-STEAM with synchronized breathing (CV = 12.2%) was slightly higher than for MC-STEAM with synchronized breathing (CV = 9.6%) and intra-session variability of UI was much larger for VAPOR-STEAM (CV = 51.7%) than for MC-STEAM (CV = 17.2%). These higher variabilities could likely be explained by less robust phase and frequency corrections in the case of VAPOR-STEAM, due to the low SNR of the lipid signals in the individual acquisitions. However, liver lipid content as determined by VAPOR-STEAM and MC-STEAM over all measurements did not significantly differ.

The inter-session variability of liver lipid content quantification was better for MC-STEAM (CV = 23.2% and 29.4% for free and synchronized breathing, respectively) than for VAPOR-STEAM (CV = 37.1% and 39.5% for free and synchronized breathing, respectively), but was relatively poor as compared with previous studies (CV < 10%) (Johnson et al, 2008), (Szczepaniak et al, 2005), (Thomas et al, 2005), (Van Werven et al, 2009). However, in most of those studies (Johnson et al, 2008), (Szczepaniak et al, 2005), (Thomas et al, 2005), variability was determined on the same day and all of them included obese subjects with fatty livers. In the present study, subjects were scanned twice on two separate days, approximately one week apart, and all subjects had liver lipid contents lower than 4%. Therefore small absolute differences can already result in large relative differences and part of the inter-session variability in the current may also be explained by real, biological differences in liver lipid content between the two sessions, because conditions, such as nutrition and physical activity, were not standardized. This is corroborated by a previous study showing that the variability of liver lipid content over one month was significantly greater than the within-day reproducibility (CV = 44% vs. 7% in subjects without diabetes) (Stephenson et al, 2013). Moreover, it has been demonstrated that both diet and exercise affect liver lipid content (Cheng et al, 2017), (Shah et al, 2009).

The unsaturation index (UI) of hepatic lipids, as determined from the MC-STEAM measurements, was found to be negatively correlated with liver lipid content, even though the liver lipid contents of our subjects all fall in a very narrow range. This is in agreement with previous findings that UI decreases with liver lipid content in NAFLD patients (Puri et al, 2007), (Hamilton et al, 2020) and in healthy subjects with a broad range of liver lipid contents (Gajdosik et al, 2015), and extends the relationship also to the regime of very low liver lipid contents.

In conclusion, non-water suppressed MC-STEAM at a 7 T system with parallel transmit is a promising approach for ^{1}H-MRS applications in the body which are affected by motion, such as in the liver. Robust phase and frequency correction of individual acquisitions before averaging, enabled by the preserved water signal in MC-STEAM, yields better repeatability and reproducibility compared with water-suppressed measurements.

5. CONCLUSION

In this research we were able perform an ex-vivo study using a mice model of NALFD that resemble the human disease. We developed a method to classify the fatty liver disease into its main three categories (healthy, steatosis and NASH) by using MRS. With these results we validate a non-invasive technique that could replace in the future the actual gold standard to perform that categorization, which is the liver biopsy.

Then, we progressed to an in-vivo analysis validated by an ex-vivo study. In this case we use mice model fed with a CDAA diet, in order to also analyse the impact of different diets.

Finally, we performed a translational study with human volunteers, by using MRS at a 7 T equipment, in order to evaluate whether it would be possible to identify and quantify all the peaks analysed in the mice models, in the in-vivo MR spectrum.

The mainly results of this study allow us to reach the following conclusions:

Ex-vivo study using mice fed with Western diet

1. There is a significant decrease in polyunsaturated fatty acids during the progression of the NAFLD from steatosis to NASH, and this decrease can be appreciated in the peak 2.8 ppm from the MRS results and from the following fatty acids (mainly) in the GC-MS results: C20:4, C22:6.
2. The results found in CG-MS validated the results found by MRS.
3. It is possible to use the principal component analysis with the seven peaks found in the MRS to classify the stages of the NALFD (healthy, steatosis and NASH).

Ex-vivo and in-vivo study using mice fed with CDAA diet

4. During different stages of NASH, we cannot appreciate changes in fatty acids in MRS and this conclusion was validated by the CG-MS.
5. The results in-vivo and ex-vivo were the same for 5/7 of the total peaks, however the Allylic and Diallylic peak presented some differences; however, less the 1%. This could be explained by the noise interference in the in-vivo results, as they are the smaller peaks. Also, in the case of in-vivo results, the allylic peak overlaps with

α-methylene and could lead to a not optimal fitting, then a not exactly correct result.

6. The ex-vivo analysis was essential to validate the results with the GC-MS and the histology and helped to understand the trend of the in-vivo analysis, since the metabolites percentual had some differences.
7. The in-vivo analysis showed to be extremely useful in order to follow each subject during time.

In-vivo study with volunteers

8. We were able to identify and quantify all the 7 peaks correspondent to fatty acids in human being, even with healthy subjects that had less than 5% of fat in the liver.
9. The method applied in this study, the MC-STEAM at a 7 T system with parallel transmit, showed to be a promising approach for ^{1}H-MRS applications in the body which are affected by motion, such as in the liver.

Future work:

1- To analyse the fatty acids composition during the progression of NALFD comparing male and female, also different hormonal stages (fertile and menopause).

2- We have characterized the fatty acids using MRS with two different types of diet (Western and CDAA), however it would be interesting to have a bigger quantity of diets, including different stages of the disease.

3- In our last study, with volunteers, we were able to analyse only healthy people, however it would be essential to increase the sample to add people with steatosis and NASH in order to validate the method. Unfortunately, this comes with big ethical difficulties since for validation of the method it is necessary the biopsy of all these patients. Besides that, in order to translate this method to clinical use, it would be necessary that the 7 Tesla was approved to be used clinically or translate this method to 3 Tesla and deal with all the complications of low spectral resolution at low fields.

BIBLIOGRAFIA

1. Ahmed, M. (2015). Non-alcoholic fatty liver disease in 2015. *World journal of hepatology*, *7*(11), 1450.
2. An, L., Willem van der Veen, J., Li, S., Thomasson, D. M., & Shen, J. (2013). Combination of multichannel single-voxel MRS signals using generalized least squares. *Journal of Magnetic Resonance Imaging*, *37*(6), 1445-1450.
3. Angulo, P. (2002). Nonalcoholic fatty liver disease. *New England Journal of Medicine*, *346*(16), 1221-1231.
4. Araya, J., Rodrigo, R., Videla, L. A., Thielemann, L., Orellana, M., Pettinelli, P., & Poniachik, J. (2004). Increase in long-chain polyunsaturated fatty acid n− 6/n− 3 ratio in relation to hepatic steatosis in patients with non-alcoholic fatty liver disease. *Clinical science*, *106*(6), 635-643.
5. Bazan, N. G. (2005). Neuroprotectin D1 (NPD1): a DHA-derived mediator that protects brain and retina against cell injury-induced oxidative stress. *Brain pathology*, *15*(2), 159-166.
6. Bannenberg, G., Arita, M., & Serhan, C. N. (2007). Endogenous receptor agonists: resolving inflammation. *The Scientific World Journal*, *7*, 1440-1462.
7. Buechler, C., & Aslanidis, C. (2020). Role of lipids in pathophysiology, diagnosis and therapy of hepatocellular carcinoma. *Biochimica et Biophysica Acta (BBA)-Molecular and Cell Biology of Lipids*, 158658.
8. Claridge, T. D. (2016). *High-resolution NMR techniques in organic chemistry* (Vol. 27). Elsevier.
9. Cabrera, D., Wree, A., Povero, D., Solís, N., Hernandez, A., Pizarro, M., ... & Brandan, E. (2017). Andrographolide ameliorates inflammation and fibrogenesis and attenuates inflammasome activation in experimental non-alcoholic steatohepatitis. *Scientific reports*, *7*(1), 1-12.
10. Cheng, S., Ge, J., Zhao, C., Le, S., Yang, Y., Ke, D., ... & Sun, J. (2017). Effect of aerobic exercise and diet on liver fat in pre-diabetic patients with non-alcoholic-fatty-liver-disease: a randomized controlled trial. *Scientific reports*, *7*(1), 1-11.

11. Cohen, J. C., Horton, J. D., & Hobbs, H. H. (2011). Human fatty liver disease: old questions and new insights. *Science*, *332*(6037), 1519-1523.
12. De Graaf, R. A. (2019). *In vivo NMR spectroscopy: principles and techniques*. John Wiley & Sons.
13. De Graaf, R. A., Sacolick, L. I., & Rothman, D. L. (2006). Water and metabolite-modulated MR spectroscopy and spectroscopic imaging. In *Proceedings of the 14th Annual Meeting of ISMRM, Seattle, Washington, USA* (p. 3063).
14. Dixon, W. T. (1984). Simple proton spectroscopic imaging. *Radiology*, *153*(1), 189-194.
15. Dreher, W., & Leibfritz, D. (2005). New method for the simultaneous detection of metabolites and water in localized in vivo 1H nuclear magnetic resonance spectroscopy. *Magnetic Resonance in Medicine: An Official Journal of the International Society for Magnetic Resonance in Medicine*, *54*(1), 190-195.
16. Elizondo, A., Araya, J., Rodrigo, R., Poniachik, J., Csendes, A., Maluenda, F., ... & Videla, L. A. (2007). Polyunsaturated fatty acid pattern in liver and erythrocyte phospholipids from obese patients. *Obesity*, *15*(1), 24-31.
17. Fillmer, A., Hock, A., Cameron, D., & Henning, A. (2017). Non-Water-Suppressed 1 H MR Spectroscopy with Orientational Prior Knowledge Shows Potential for Separating Intra-and Extramyocellular Lipid Signals in Human Myocardium. *Scientific reports*, *7*(1), 1-14.
18. Fillmer, A., Castro, C. A., Xavier, A., Luijten, P. R., Klomp, D. W., & Prompers, J. J. (2019). Implementation of metabolite cycled liver 1H MRS on a 7T parallel transmit system. *In Proceeding of the of the 27th Annual Meeting of ISMRM, Montreal, Quebec, Canada* (n. 4232).
19. Fillmer, A., Kirchner, T., Cameron, D., & Henning, A. (2015). Constrained image-based B0 shimming accounting for “local minimum traps” in the optimization and field inhomogeneities outside the region of interest. *Magnetic resonance in medicine*, *73*(4), 1370-1380.
20. Friedman, S. L., Neuschwander-Tetri, B. A., Rinella, M., & Sanyal, A. J. (2018). Mechanisms of NAFLD development and therapeutic strategies. *Nature medicine*, *24*(7), 908-922.

21. Folch, J., Lees, M., & Stanley, G. S. (1957). A simple method for the isolation and purification of total lipides from animal tissues. *Journal of biological chemistry*, *226*(1), 497-509.
22. Gajdošík, M., Chadzynski, G. L., Hangel, G., Mlynárik, V., Chmelík, M., Valkovič, L., ... & Krššák, M. (2015). Ultrashort-TE stimulated echo acquisition mode (STEAM) improves the quantification of lipids and fatty acid chain unsaturation in the human liver at 7 T. *NMR in Biomedicine*, *28*(10), 1283-1293.
23. Gajdošík, M., Chmelík, M., Just-Kukurová, I., Bogner, W., Valkovič, L., Trattnig, S., & Krššák, M. (2014). In vivo relaxation behavior of liver compounds at 7 tesla, measured by single-voxel proton MR spectroscopy. *Journal of Magnetic Resonance Imaging*, *40*(6), 1365-1374.
24. Giapitzakis, I. A., Shao, T., Avdievich, N., Mekle, R., Kreis, R., & Henning, A. (2018). Metabolite-cycled STEAM and semi-LASER localization for MR spectroscopy of the human brain at 9.4 T. *Magnetic resonance in medicine*, *79*(4), 1841-1850.
25. Guillén, M. D., & Ruiz, A. (2003). Edible oils: discrimination by 1H nuclear magnetic resonance. *Journal of the Science of Food and Agriculture*, *83*(4), 338-346.
26. Hansen, H. H., Feigh, M., Veidal, S. S., Rigbolt, K. T., Vrang, N., & Fosgerau, K. (2017). Mouse models of nonalcoholic steatohepatitis in preclinical drug development. *Drug discovery today*, *22*(11), 1707-1718.
27. Hariri, N., & Thibault, L. (2010). High-fat diet-induced obesity in animal models. *Nutrition research reviews*, *23*(2), 270-299.
28. Hamilton, G., Yokoo, T., Bydder, M., Cruite, I., Schroeder, M. E., Sirlin, C. B., & Middleton, M. S. (2011). In vivo characterization of the liver fat 1H MR spectrum. *NMR in biomedicine*, *24*(7), 784-790.
29. Hebbard, L., & George, J. (2011). Animal models of nonalcoholic fatty liver disease. *Nature reviews Gastroenterology & hepatology*, *8*(1), 35.
30. Hirsova, P., & Gores, G. J. (2015). Death receptor-mediated cell death and proinflammatory signaling in nonalcoholic steatohepatitis. *Cellular and molecular gastroenterology and hepatology*, *1*(1), 17-27.

31. Hock, A., MacMillan, E. L., Fuchs, A., Kreis, R., Boesiger, P., Kollias, S. S., & Henning, A. (2013). Non-water-suppressed proton MR spectroscopy improves spectral quality in the human spinal cord. *Magnetic resonance in medicine*, *69*(5), 1253-1260.
32. Hwang, T. L., Van Zijl, P. C., & Garwood, M. (1999). Asymmetric adiabatic pulses for NH selection.
33. James, G., Witten, D., & Hastie, T. (2013). &Robert Tibshirani,"An Introduction to Statistical Learning".
34. Jiménez-Xarrié, E., Davila, M., Gil-Perotín, S., Jurado-Rodríguez, A., Candiota, A. P., Delgado-Mederos, R., ... & Martí-Fàbregas, J. (2015). In vivo and ex vivo magnetic resonance spectroscopy of the infarct and the subventricular zone in experimental stroke. *Journal of Cerebral Blood Flow & Metabolism*, *35*(5), 828-834.
35. Johnson, N. A., Walton, D. W., Sachinwalla, T., Thompson, C. H., Smith, K., Ruell, P. A., ... & George, J. (2008). Noninvasive assessment of hepatic lipid composition: advancing understanding and management of fatty liver disorders. *Hepatology*, *47*(5), 1513-1523.
36. Kleiner, D. E., Brunt, E. M., Van Natta, M., Behling, C., Contos, M. J., Cummings, O. W., ... & Yeh, M. (2005). Design and validation of a histological scoring system for nonalcoholic fatty liver disease. *Hepatology*, *41*(6), 1313-1321.
37. Knothe, G., & Kenar, J. A. (2004). Determination of the fatty acid profile by 1H-NMR spectroscopy. *European Journal of Lipid Science and Technology*, *106*(2), 88-96.
38. Krishnan, A., Abdullah, T. S., Mounajjed, T., Hartono, S., McConico, A., White, T., ... & Charlton, M. (2017). A longitudinal study of whole body, tissue, and cellular physiology in a mouse model of fibrosing NASH with high fidelity to the human condition. *American Journal of Physiology-Gastrointestinal and Liver Physiology*, *312*(6), G666-G680.
39. Lau, J. K. C., Zhang, X., & Yu, J. (2017). Animal models of non-alcoholic fatty liver disease: current perspectives and recent advances. *The Journal of pathology*, *241*(1), 36-44.
40. Lee, Y., Jee, H. J., Noh, H., Kang, G. H., Park, J., Cho, J., ... & Oh, B. C. (2013). In vivo 1H-MRS hepatic lipid profiling in nonalcoholic fatty liver disease: An animal study at 9.4 T. *Magnetic resonance in medicine*, *70*(3), 620-629.

41. Leporq, B., Lambert, S. A., Ronot, M., Vilgrain, V., & Van Beers, B. E. (2014). Quantification of the triglyceride fatty acid composition with 3.0 T MRI. *NMR in Biomedicine*, *27*(10), 1211-1221.
42. Levant, B., Ozias, M. K., Guilford, B. L., & Wright, D. E. (2013). Streptozotocin-induced diabetes partially attenuates the effects of a high-fat diet on liver and brain fatty acid composition in mice. *Lipids*, *48*(9), 939-948.
43. Longato, L. (2013). Non-alcoholic fatty liver disease (NAFLD): a tale of fat and sugar?. *Fibrogenesis & tissue repair*, *6*(1), 14.
44. Longo, R., Pollesello, P., Ricci, C., Masutti, F., Kvam, B. J., Bercich, L., ... & Tiribelli, C. (1995). Proton MR spectroscopy in quantitative in vivo determination of fat content in human liver steatosis. *Journal of Magnetic Resonance Imaging*, *5*(3), 281-285.
45. Lundbom, J., Hakkarainen, A., Söderlund, S., Westerbacka, J., Lundbom, N., & Taskinen, M. R. (2011). Long-TE 1H MRS suggests that liver fat is more saturated than subcutaneous and visceral fat. *NMR in Biomedicine*, *24*(3), 238-245.
46. MacMillan, E. L., Chong, D. G., Dreher, W., Henning, A., Boesch, C., & Kreis, R. (2011). Magnetization exchange with water and T1 relaxation of the downfield resonances in human brain spectra at 3.0 T. *Magnetic resonance in medicine*, *65*(5), 1239-1246.
47. Machado, M. V., Michelotti, G. A., Xie, G., de Almeida, T. P., Boursier, J., Bohnic, B., ... & Diehl, A. M. (2015). Mouse models of diet-induced nonalcoholic steatohepatitis reproduce the heterogeneity of the human disease. *PloS one*, *10*(5).
48. Metzger, G. J., Snyder, C., Akgun, C., Vaughan, T., Ugurbil, K., & Van de Moortele, P. F. (2008). Local B1+ shimming for prostate imaging with transceiver arrays at 7T based on subject-dependent transmit phase measurements. *Magnetic Resonance in Medicine: An Official Journal of the International Society for Magnetic Resonance in Medicine*, *59*(2), 396-409.
49. McClain, C. J., Barve, S., & Deaciuc, I. (2007). Good fat/bad fat. *Hepatology*, *45*(6), 1343-1346.
50. Miyake, Y., Yokomizo, K., & Matsuzaki, N. (1998). Determination of unsaturated fatty acid composition by high-resolution nuclear magnetic resonance spectroscopy. *Journal of the American Oil Chemists' Society*, *75*(12), 1091-1094.

51. Neuman, M. G., Cohen, L. B., & Nanau, R. M. (2014). Biomarkers in nonalcoholic fatty liver disease. *Canadian Journal of Gastroenterology and Hepatology*, *28*(11), 607-618.
52. Peereboom, S. M., Gastl, M., Fuetterer, M., & Kozerke, S. (2020). Navigator-free metabolite-cycled proton spectroscopy of the heart. *Magnetic resonance in medicine*, *83*(3), 795-805.
53. Permutt, Z., Le, T. A., Peterson, M. R., Seki, E., Brenner, D. A., Sirlin, C., & Loomba, R. (2012). Correlation between liver histology and novel magnetic resonance imaging in adult patients with non-alcoholic fatty liver disease–MRI accurately quantifies hepatic steatosis in NAFLD. *Alimentary pharmacology & therapeutics*, *36*(1), 22-29.
54. Perry, R. J., Zhang, D., Zhang, X. M., Boyer, J. L., & Shulman, G. I. (2015). Controlled-release mitochondrial protonophore reverses diabetes and steatohepatitis in rats. *Science*, *347*(6227), 1253-1256.
55. Poole, R. K. (2008). Globins and other nitric oxide-reactive proteins.
56. Puri, P., Baillie, R. A., Wiest, M. M., Mirshahi, F., Choudhury, J., Cheung, O., ... & Sanyal, A. J. (2007). A lipidomic analysis of nonalcoholic fatty liver disease. *Hepatology*, *46*(4), 1081-1090.
57. Raaijmakers, A. J., Italiaander, M., Voogt, I. J., Luijten, P. R., Hoogduin, J. M., Klomp, D. W., & van Den Berg, C. A. (2016). The fractionated dipole antenna: A new antenna for body imaging at 7 T esla. *Magnetic resonance in medicine*, *75*(3), 1366-1374.
58. Reeder, S. B., Cruite, I., Hamilton, G., & Sirlin, C. B. (2011). Quantitative assessment of liver fat with magnetic resonance imaging and spectroscopy. *Journal of magnetic resonance imaging*, *34*(4), 729-749.
59. Ren, J., Dimitrov, I., Sherry, A. D., & Malloy, C. R. (2008). Composition of adipose tissue and marrow fat in humans by 1H NMR at 7 Tesla. *Journal of lipid research*, *49*(9), 2055-2062.
60. Sanches, S. C. L., Ramalho, L. N. Z., Augusto, M. J., da Silva, D. M., & Ramalho, F. S. (2015). Nonalcoholic steatohepatitis: a search for factual animal models. *BioMed research international*, *2015*.

61. Shah, K., Stufflebam, A., Hilton, T. N., Sinacore, D. R., Klein, S., & Villareal, D. T. (2009). Diet and exercise interventions reduce intrahepatic fat content and improve insulin sensitivity in obese older adults. *Obesity*, *17*(12), 2162-2168.
62. Stefan, D. D. C. F., Di Cesare, F., Andrasescu, A., Popa, E., Lazariev, A., Vescovo, E., ... & Van Ormondt, D. (2009). Quantitation of magnetic resonance spectroscopy signals: the jMRUI software package. *Measurement Science and Technology*, *20*(10), 104035.
63. Steensma, B. R., Voogt, I. J., Leiner, T., Luijten, P. R., Habets, J., Klomp, D. W., ... & Raaijmakers, A. J. (2018). An 8-channel Tx/Rx dipole array combined with 16 Rx loops for high-resolution functional cardiac imaging at 7 T. *Magnetic Resonance Materials in Physics, Biology and Medicine*, *31*(1), 7-18.
64. Stephenson, M. C., Leverton, E., Khoo, E. Y. H., Poucher, S. M., Johansson, L., Lockton, J. A., ... & MacDonald, I. A. (2013). Variability in fasting lipid and glycogen contents in hepatic and skeletal muscle tissue in subjects with and without type 2 diabetes: a 1H and 13C MRS study. *NMR in Biomedicine*, *26*(11), 1518-1526.
65. Szczepaniak, L. S., Nurenberg, P., Leonard, D., Browning, J. D., Reingold, J. S., Grundy, S., ... & Dobbins, R. L. (2005). Magnetic resonance spectroscopy to measure hepatic triglyceride content: prevalence of hepatic steatosis in the general population. *American Journal of Physiology-Endocrinology and Metabolism*, *288*(2), E462-E468.
66. Tetri, L. H., Basaranoglu, M., Brunt, E. M., Yerian, L. M., & Neuschwander-Tetri, B. A. (2008). Severe NAFLD with hepatic necroinflammatory changes in mice fed trans fats and a high-fructose corn syrup equivalent. *American Journal of Physiology-Gastrointestinal and Liver Physiology*, *295*(5), G987-G995.
67. Thomas, E. L., Hamilton, G., Patel, N., O'Dwyer, R., Doré, C. J., Goldin, R. D., ... & Taylor-Robinson, S. D. (2005). Hepatic triglyceride content and its relation to body adiposity: a magnetic resonance imaging and proton magnetic resonance spectroscopy study. *Gut*, *54*(1), 122-127.
68. Tkáč, I., Starčuk, Z., Choi, I. Y., & Gruetter, R. (1999). In vivo 1H NMR spectroscopy of rat brain at 1 ms echo time. *Magnetic Resonance in Medicine: An Official Journal of the International Society for Magnetic Resonance in Medicine*, *41*(4), 649-656.

69. Tilg, H., & Moschen, A. R. (2010). Evolution of inflammation in nonalcoholic fatty liver disease: the multiple parallel hits hypothesis. *Hepatology*, *52*(5), 1836-1846.
70. Van Herck, M. A., Vonghia, L., & Francque, S. M. (2017). Animal models of nonalcoholic fatty liver disease—a starter's guide. *Nutrients*, *9*(10), 1072.
71. van Werven, J. R., Hoogduin, J. M., Nederveen, A. J., van Vliet, A. A., Wajs, E., Vandenberk, P., ... & Stoker, J. (2009). Reproducibility of 3.0 Tesla magnetic resonance spectroscopy for measuring hepatic fat content. *Journal of Magnetic Resonance Imaging: An Official Journal of the International Society for Magnetic Resonance in Medicine*, *30*(2), 444-448.
72. Vanhamme, L., van den Boogaart, A., & Van Huffel, S. (1997). Improved method for accurate and efficient quantification of MRS data with use of prior knowledge. *Journal of magnetic resonance*, *129*(1), 35-43.
73. Wang, X., Cao, Y., Fu, Y., Guo, G., & Zhang, X. (2011). Liver fatty acid composition in mice with or without nonalcoholic fatty liver disease. *Lipids in health and disease*, *10*(1), 234.
74. Ward Jr, J. H. (1963). Hierarchical grouping to optimize an objective function. *Journal of the American statistical association*, *58*(301), 236-244.
75. Wiegers, E. C., Philips, B. W., Heerschap, A., & van der Graaf, M. (2017). Automatic frequency and phase alignment of in vivo J-difference-edited MR spectra by frequency domain correlation. *Magnetic Resonance Materials in Physics, Biology and Medicine*, *30*(6), 537-544.
76. Williams, R., & Taylor-Robinson, S. D. (2016). *Clinical dilemmas in non-alcoholic fatty liver disease*. John Wiley & Sons.
77. Wilson, M., Davies, N. P., Grundy, R. G., & Peet, A. C. (2009). A quantitative comparison of metabolite signals as detected by in vivo MRS with ex vivo 1H HR-MAS for childhood brain tumours. *NMR in Biomedicine: An International Journal Devoted to the Development and Application of Magnetic Resonance In vivo*, *22*(2), 213-219.
78. Xavier, A., Zacconi, F., Cabrera, D., Fuenzalida, K., & Andia, M. (2019). Hepatic Fatty Acid Profile in Mice with Nonalcoholic Fatty Liver Disease Using Magnetic Resonance Spectroscopy. In: Costa-Felix R., Machado J., Alvarenga A. (eds) XXVI

Brazilian Congress on Biomedical Engineering. *IFMBE Proceedings*, 70(1). Springer, Singapore.

79. Xavier, A., Zacconi, F., Gainza, C., Cabrera, D., Arrese, M., Uribe, S., ... & Andia, M. E. (2019). Intrahepatic fatty acids composition as a biomarker of NAFLD progression from steatosis to NASH by using ^{1}H-MRS. *RSC Advances*, *9*(72), 42132-42139.
80. Xavier, A., Zacconi, F., Eykyn, Plaza, B., Phinikaridou, A., & Andia, M.E (2019). In vivo and ex vivo quantification of hepatic fatty acid in mice fed with CDAA-diet using magnetic resonance spectroscopy at 9.4 T. *In Proceeding of the of the 36th Annual Meeting of ESMRMB, Rotterdam, The Netherlands*, (S55).
81. Xavier, A., Arteaga de Castro, C.S., Andia, M.E., Luijten, P. R., Klomp, D. W., Fillmer, A., and Prompers, J.J. (2020) Metabolite cycled liver ^{1}H MRS on a 7 T parallel transmit system. *NMR Biomed*, 33, E4343.
82. Xavier, A., Zacconi, F. C., Santana-Romo, F., Eykyn, T., Lavin-Plaza, B., Phinikaridou, A., Botnar, R., Uribe, S., Oyarzún, J.E., Cabrera, D., Arrese, M., Andia. M.E. Intrahepatocyte fatty acids characterization in a mice model during NASH progression using in vivo and ex vivo magnetic resonance spectroscopy. [under review]
83. Yamada, K., Mizukoshi, E., Sunagozaka, H., Arai, K., Yamashita, T., Takeshita, Y., ... & Nakanuma, Y. (2015). Characteristics of hepatic fatty acid compositions in patients with nonalcoholic steatohepatitis. *Liver International*, *35*(2), 582-590.
84. Yarnykh, V. L. (2007). Actual flip-angle imaging in the pulsed steady state: a method for rapid three-dimensional mapping of the transmitted radiofrequency field. *Magnetic Resonance in Medicine: An Official Journal of the International Society for Magnetic Resonance in Medicine*, *57*(1), 192-200.
85. Younossi, Z. M., Koenig, A. B., Abdelatif, D., Fazel, Y., Henry, L., & Wymer, M. (2016). Global epidemiology of nonalcoholic fatty liver disease—meta-analytic assessment of prevalence, incidence, and outcomes. *Hepatology*, *64*(1), 73-84.
86. Younossi, Z., Stepanova, M., Ong, J. P., Jacobson, I. M., Bugianesi, E., Duseja, A., ... & Romero-Gomez, M. (2019). Nonalcoholic steatohepatitis is the fastest growing cause of hepatocellular carcinoma in liver transplant candidates. *Clinical Gastroenterology and Hepatology*, *17*(4), 748-755.
87. Yurkanis Bruice, P. (2008). Química orgánica.